GEOFLUIDS

Geofluids (2010) **10**, 142–160 doi: 10.1111/j.1468-8123.2009.00274.x

Using seafloor heat flow as a tracer to map subseafloor fluid flow in the ocean crust

A. T. FISHER[1] AND R. N. HARRIS[2]

[1]*Earth and Planetary Sciences Department and Institute for Geophysics and Planetary Physics, University of California, Santa Cruz, Santa Cruz, CA, USA;* [2]*College of Oceanic and Atmospheric Sciences, Oregon State University, Corvallis, OR, USA*

ABSTRACT

We describe how seafloor heat flow is determined, review current understanding of advective heat loss from oceanic lithosphere, and present results from three field areas to illustrate how heat flow measurements are used (along with complementary data) to resolve fluid flow rates and patterns. Conductive heat flow through much of the seafloor is lower than predicted by lithospheric cooling models as a result of hydrothermal circulation; this discrepancy is the basis for global estimates of the magnitude of advective cooling of oceanic lithosphere. Hydrothermal circulation also redistributes heat within the ocean crustal aquifer, leading to local variability. Heat flow studies in Middle Valley, a sedimented spreading center in the northeastern Pacific Ocean, indicate multiple scales of fluid circulation, delineate conditions at the top of a hydrothermal reservoir, and show the influence of primary and secondary convection. Heat flow studies on the eastern flank of the Juan de Fuca Ridge document the thermal influence of isolated basement outcrops surrounded by thick, low-permeability sediments. Warm hydrothermal fluids seep from the crust through a small volcanic edifice, having flowed into the crust through a larger outcrop ~50 km to the south. These fluids generate a local geothermal anomaly, but have little influence on regional heat loss from the plate. In contrast, heat flow surveys on part of the Cocos Plate, eastern Equatorial Pacific Ocean, indicate that regional conductive heat loss is just 10–40% of predictions from lithospheric cooling models. Basement outcrops in this area focus massive discharge of cool, hydrothermal fluid and associated heat ($4–80 \times 10^3$ l s^{-1} of fluid, 0.8–1.4 GW of heat). Seafloor heat flow studies will be increasingly important in coming years for understanding marine hydrogeologic regimes and the role of fluids in a variety of Earth processes and settings.

Key words: seafloor heat flow, subseafloor fluid flow, hydrothermal systems, modeling

Received 29 July 2009; accepted 7 November 2009

Corresponding author: A. T. Fisher, Earth and Planetary Sciences Department and Institute for Geophysics and Planetary Physics, University of California, Santa Cruz, Santa Cruz, CA 95064, USA.
Email: afisher@ucsc.edu. Tel.: +831 459 5598. Fax: +831 459 3074.

Geofluids (2010) **10**, 142–160

INTRODUCTION

Soon after collection of the first oceanographic heat flow data (Bullard 1954; Revelle & Maxwell 1952), it was recognized that seafloor heat flow was generally highest and most variable near mid-ocean ridges, areas of elevated basement rocks that lacked thick and continuous sediment cover. At the time when initial heat flow data were collected, theories of seafloor spreading and plate tectonics were not fully developed or widely accepted, and there was considerable debate as to how heat flow measurements should be interpreted (Elder 1965; Langseth *et al.* 1966; Sclater 2004). Once convincing evidence for seafloor spreading became apparent, heat flow data presented a conundrum. It was expected that the oceanic lithosphere should release the most heat near spreading centers where the seafloor is youngest (McKenzie 1967; Lister 1972; Parker & Oldenberg 1973), but the variable heat flow seen at young sites commonly included low heat flow values. The difference between theory and observation was resolved by the realization that seafloor heat flow measurements, which document the conductive portion of lithospheric heat loss, generally do not measure the heat that is removed advectively by hydrothermal circulation. In addition,

hydrothermal circulation helps to explain the variability commonly observed in regional heat flow surveys, which can result in local redistribution of heat within the crust (whether or not there is net advective heat loss).

Theoretical seafloor cooling curves were developed initially in the late 1960s, and have been refined and extended in decades hence, using bathymetric and heat flow data to constrain the physical properties and evolution of oceanic lithosphere as plates age (Davis & Lister 1974; Parsons & Sclater 1977; Stein & Stein 1992). These cooling curves are important for quantifying the magnitude of the conductive heat flow deficit associated with advective heat loss, the extent of local heat redistribution within the lithosphere, the suppression of seafloor heat flow by rapid sedimentation, and other geologic and hydrologic processes (e.g., Anderson & Hobart 1976; Sclater *et al.* 1980; Davis *et al.* 1989; Wang & Davis 1992).

The last 10–15 years has seen renewed interest in using seafloor heat flow to resolve marine hydrogeologic processes, contemporaneous with increasing application of heat as a tracer in surface water and ground water studies on land (e.g., Anderson 2005; Burow *et al.* 2005; Constantz *et al.* 2001). Heat offers many advantages as a tracer of fluid flow. Variations in fluid temperature and heat flow occur naturally within many hydrogeologic systems and at a range of spatial and temporal time scales. Water has a high heat capacity, so relatively small rates of fluid flow can result in significant thermal perturbations. The long-term consistency of bottom water temperatures in the deep ocean imposes a stable boundary condition at the seafloor in many areas, simplifying the application of coupled fluid–thermal flow models. Recent technical advances have made collection of seafloor thermal data easier, cheaper, and more reliable, accurate and precise. Finally, improvements and standardization in ship and instrument navigation allow co-location of complementary mapping, seismic, and chemical data, providing a broader geological context for interpretation of thermal data.

In this paper, we review the basis for marine heat flow data collection and processing, and discuss how these data are used to quantify rates and patterns of fluid flow. We discuss thermal data and interpretations based on global data summaries and regional studies of three geologic settings to illustrate key concepts. There are many hydrogeologic settings where researchers have used heat to quantify fluid flow using water column, seafloor, and subseafloor tools, including studies based on transient variations in shallow heat flow (e.g., Becker *et al.* 1983, 1995; Kinoshita *et al.* 1996; Veirs *et al.* 1999; Goto *et al.* 2005; Hamamoto *et al.* 2005). Space limitations preclude a comprehensive presentation of these topics; instead, we highlight studies of rapid lateral fluid flow in permeable volcanic rocks of the upper oceanic crust using shallow heat flow measurement surveys.

METHODS

Theoretical basis

Seafloor heat flow measurements are based on application of a simplified form of Fourier's first law for vertical heat transport:

$$q = -\lambda \frac{\mathrm{d}T}{\mathrm{d}z} \tag{1}$$

where q = heat flow (W m^{-2}), λ = thermal conductivity (W m^{-1} °C^{-1}), and $\mathrm{d}T/\mathrm{d}z$ = thermal gradient (°C m^{-1}). Thus determining the conductive seafloor heat flow requires measurements of both the thermal conductivity and the thermal gradient. The negative sign on the right-hand side of Eq. (1) indicates that heat flows in a direction opposite to the thermal gradient.

In fact, Fourier's first law is a special case of a more general, one-dimensional transient, conduction equation:

$$\frac{\partial}{\partial z}\left(\kappa \frac{\partial T}{\partial z}\right) = \frac{\partial T}{\partial t} \tag{2}$$

where κ is the thermal diffusivity, the ratio of thermal conductivity to heat capacity. It is often assumed that heat flow through the top of a thermal boundary layer (such as most marine sediments) occurs at steady state, so that the right-hand side of Eq. (2) is set to zero. However, the thermal diffusivity can change with depth, leading to variations in the thermal gradient, even when heat flow is purely conductive (as discussed later).

If there is also heat advection by fluid, the one-dimensional transient equation becomes:

$$\frac{\partial}{\partial z}\left(\kappa \frac{\partial T}{\partial z}\right) - \frac{n v_\mathrm{f}}{\gamma}\frac{\partial T}{\partial z} = \frac{\partial T}{\partial t} \tag{3}$$

where n = layer porosity, v_f = fluid velocity (nv_f is volume flux/area = specific discharge), and γ = the ratio of fluid and saturated formation heat capacities. As a practical matter, it is difficult to resolve the fluid velocity through seafloor materials independent of Eq. (3), so a form of this equation is sometimes used to estimate the fluid flow rate from thermal observations.

Equation (3) is one-dimensional, vertical, and based on a constant fluid flow rate. Fluid and heat transport in many seafloor hydrogeologic systems are transient, occur in two or three dimensions, and are fully coupled. Modeling of systems having these complexities may require more sophisticated analytical or numerical approaches, especially if there are spatial or temporal changes in fluid and formation

properties, reactive transport, or other non-linear links between fluid and heat flow.

Data collection

Seafloor heat flow measurements are made in marine sediments with two primary kinds of tools: (i) instruments that penetrate the seafloor and determine temperatures within shallow sediments (generally <10 m) and (ii) instruments deployed within sediments while drilling to greater depths (~30–400 m). Examples of these tools and their use are summarized briefly in this section.

Multipenetration probes comprise a weight stand and data logger, a lance that holds thermal sensors, and a telemetry system that sends data from the seafloor to the surface (Fig. 1A) (Langseth *et al.* 1965; Davis 1988). Most

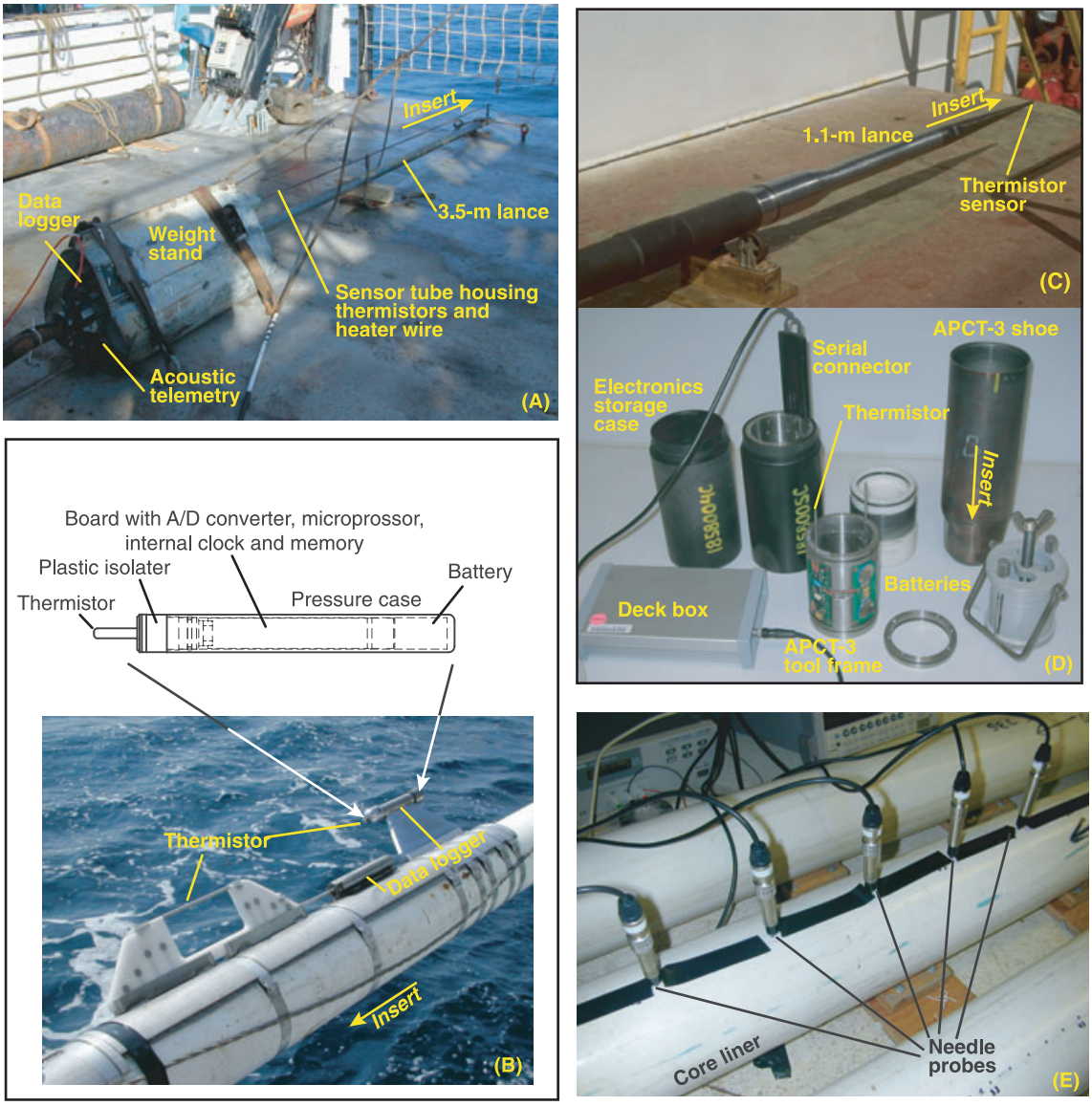

Fig. 1. Examples of seafloor heat flow instrumentation used in marine sediments above a basement aquifer. Arrows labeled ''*Insert*'' in panels A–D indicate orientation of instruments when pushed into the seafloor. See text for description and citations for more information on tool design, use, and limitations. (A) Violin-bow, multipenetration heat flow probe used to determine shallow gradients and in-situ thermal conductivity. (B) Autonomous outrigger probes showing construction of logger (top, sketch) and two styles of probes as deployed (bottom, photograph). Probe with fin and long-style thermistor tube (left), and probe with short sensor (right) mounted on a piston core barrel. In both cases the data logger and battery are housed inside a protective pressure case that also functions as a serial connector for programming and data download. (C) Davis–Villinger Temperature Probe used for measurement of sediment temperature at the base of a borehole. Tool (silver) is mounted inside a core barrel (dark gray) for deployment, then pushed into the sediment using the drillstring. (D) Third generation of advanced piston coring temperature tool (APCT-3) used to measure sediment temperature while piston coring with a drillship. Tool frame with thermistor probe (center bottom) is placed inside annular cavity in piston coring shoe (upper right) prior to deployment. (E) Needle probes inserted through core liner to determine the thermal conductivity of recovered sediments.

modern multipenetration systems have thermistors mounted on outrigger probes attached to a central strength member, or within a single, long 'violin bow' outrigger that positions the thermal sensors away from the central strength member (Hyndman *et al.* 1979). The precision of individual thermistor sensors is typically ±0.001°C, and probes commonly have 11 or more thermistors distributed along a 2–5 m lance. Shorter versions of these tools, often with a narrow strength member that houses the thermal sensors, are used with submersibles and remotely operated vehicles.

A multipenetration heat flow station begins with the lowering of the instrument towards the seafloor from a ship using a trawl wire and winch. The probe is driven by gravity into sediments and allowed to achieve partial equilibration with ambient formation temperatures. If the instrument has the capability to measure *in situ* thermal conductivity, a calibrated heat pulse is generated using a wire that extends along the length of the sensor tube. The temperature decay of the heat pulse provides a measure of sediment thermal conductivity at multiple depths. With the completion of a measurement, the instrument is pulled from the seafloor and hoisted 100–500 m (depending on intended measurement spacing), the ship is maneuvered to a new position, and the process is repeated. In this manner a transect of heat flow measurements can be obtained relatively quickly.

Multipenetration surveys are typically run along carefully navigated transects, often with collocated swath map and seismic data, during a deployment of 12–48 h. With some systems there is complete data telemetry, and processing can be completed in near real time. But many systems send back just enough information to evaluate tool performance and battery power, and to make a rough estimate of thermal gradients during a survey. More complete and accurate data analysis is completed after the tool is returned to the surface and data are downloaded from logger memory.

Some of the earliest oceanographic heat flow measurements were made with temperature probes attached to sediment core barrels, so that a thermal gradient could be determined at the same place and time that sediment was sampled. The technique is similar to that involving multipenetration systems, except that only one gradient is determined during each instrument lowering. Modern outrigger probes used on core barrels are robust, accurate (±0.002–0.003°C), and autonomous, recording and storing data without telemetry (Fig. 1B) (Pfender & Villinger 2002). These systems are ideal for making reconnaissance or supplemental measurements in conjunction with coring operations, which is particularly useful where sediment cover is thin or patchy. Outrigger probe systems on core barrels generally do not provide determinations of sediment thermal conductivity, so the latter measurements must be made in the laboratory using material recovered during coring (as described below). There is also a system for measuring heat flow through bare rock (Johnson & Hutnak 1996), but this tool is not widely used at present, and the vast majority of seafloor heat flow surveys are conducted on sedimented seafloor.

There are two main classes of sediment temperature probes used during scientific ocean drilling (Fisher & Becker 1993): push in tools that require a dedicated tool run, independent of coring operations (Fig. 1C) (Uyeda & Horai 1980; Davis *et al.* 1997a); and tools that are integrated with piston coring operations (Fig. 1D) (Horai & Von 1985; Fisher *et al.* 2007). These instruments are generally deployed 1–10 m beyond the drilled depth of a borehole within a few hours of drilling, avoiding the thermal (cooling) influence of pumping cold seawater as a drilling fluid.

Additional subseafloor measurements have been made during logging operations in open boreholes, either using sediment instruments on a wireline or using open hole logging instruments made specifically for this purpose (Hyndman *et al.* 1976; Becker *et al.* 1983; Fisher *et al.* 1997; Larson *et al.* 1993). Strings of thermal sensors have been deployed in subseafloor borehole observatories as part of long-term monitoring installations (e.g., Davis & Becker 1994, 2002; Foucher *et al.* 1997). Tools used during scientific ocean drilling and in boreholes are not discussed in the rest of this review, which focuses on measurements made in shallow sediments.

Thermal gradient measurements are commonly augmented with thermal conductivity measurements made in the laboratory. Even if there is *in situ* conductivity capability (as with most modern, multipenetration probes), lab measurements can be helpful because they allow more comprehensive assessment of sediment properties at a scale finer than the spacing between adjacent thermistors in a multipenetration probe or outriggers on a core barrel. The needle probe method (Fig. 1E) is most commonly used for determining the thermal conductivity of marine sediments (Von Herzen & Maxwell 1959). Marine sediments are recovered in a plastic core liner. After the core equilibrates to room temperature, a small hole is drilled in the side of the liner, and a needle probe is inserted. The probe contains a wire loop with known heating characteristics, and a thermistor is positioned near the middle of the probe. The temperature response of the probe during continuous or pulse heating through the wire allows thermal conductivity to be determined by fitting observational data to an analytical solution to a radial heat conduction equation. A modified version of this experiment can be conducted on lithified sediments or igneous rock using cut pieces of hard rock pressed against a needle that is backed with a low-conductivity substrate such as acrylic or epoxy.

Data processing

Most marine heat flow tools are not kept in the formation long enough for thermistors to fully equilibrate. Full equilibration would require more time that is commonly available, and it can be difficult to recover an instrument pushed into seafloor sediments if the formation around the tool is allowed to 'settle in' for an extended time. Instead, equilibration temperatures are computed based on model fits to ~6–8 min of temperature data, with the model response extrapolated to infinite time (Bullard & Maxwell 1956; Villinger & Davis 1987; Hartmann & Villinger 2002). Equilibration models are designed based on tool geometry and tool and formation properties. Applying these models requires some understanding of thermal conductivity because statistically equivalent fits of observations and model calculations can be achieved in many cases using a range of plausible thermal conductivity values. If *in situ* thermal conductivity data are collected, appropriate values can be assigned to individual thermistors. If no thermal conductivity data are available, values are estimated based on earlier surveys in the same (or a similar) area. In either case, Monte Carlo analysis of possible thermal conductivity variations and boundaries between layers allows assessment of uncertainties in equilibrium temperatures associated with these parameters (Stein & Fisher 2001; Hartmann & Villinger 2002).

If thermal conductivity is constant with depth, conductive vertical heat flow is calculated with Eq. (1). This equation is modified to account for changes in thermal conductivity with depth (negative sign dropped for convenience) (e.g., Bullard 1939; Louden & Wright 1989):

$$T = q \sum \frac{\Delta z}{\lambda} \tag{4}$$

where $\sum \frac{\Delta z}{\lambda}$ is the cumulative thermal resistance, and Δz is the depth interval represented by each value of λ. Conductive heat flow is calculated as the slope of a line fit through points on a plot of T versus $\sum \frac{\Delta z}{\lambda}$.

ERRORS AND UNCERTAINTIES

Inexpensive thermistor sensors can be calibrated to provide resolution and absolute accuracy of ≤0.001°C across a useful working range of 0–40°C (appropriate for thermal gradient determinations in the upper 5 m of sediment in most locations). Accurate measurements at higher temperatures are sometimes desired, especially in borehole applications, and this can be achieved through selection of thermistors having the appropriate dynamic range. Sensors are commonly calibrated in the lab using a controlled bath, or cross-calibrated in the field by holding the probe stationary in bottom water during a survey. Widely used analog-digital logger components have ≥16 bits of resolution and are extremely quiet. Thus analytical errors associated with sensors and data loggers tend to be small.

Extrapolation of partial cooling records for the sensors, and estimation of *in situ* thermal conductivity values, can lead to errors in individual temperature values of 0.01–0.05°C, even for high-quality data. The main difficulty is that equilibration records can be made to fit a variety of cooling curves depending on the assumed physical properties, which are rarely known with confidence. However, heat flow determinations are more dependent on the thermal gradient than individual temperatures, so measurement and extrapolation errors for individual sensors are likely to be greater than those for calculated thermal gradients in many cases.

When thermal conductivity is measured *in situ*, the nature and properties of materials between sensor depths may be poorly known. This is a particular problem when making measurements in thin layers of sediments having large differences in thermal properties, such as turbidites. Finally, thermal conductivity is generally not measured with a geometry that is fully consistent with vertical heat flow. *In situ* measurements determine the horizontal (radial) conductivity, whereas needle probe measurements made on sediment cores determine the geometric mean of horizontal and vertical values (Pribnow *et al.* 2000). Fortunately, anisotropy in thermal conductivity tends to be small in shallow sediments.

Although it is possible to quantify fit statistics when cross-plotting temperature and depth (or cumulative thermal resistance), this approach does not provide a conservative estimate of uncertainty in heat flow measurements. Repeated measurements made during a single instrument lowering suggest that precision is often on the order of 3–5% (Harris *et al.* 2000), but there may be additional uncertainties associated with undocumented lithologic variations, thermal refraction, or transient processes such as slumping or recent changes in bottom water temperatures. Fortunately for many applications and settings, the hydrogeologic processes inferred from thermal data often involve large differences between measured values and deviations from standard lithospheric reference curves.

The best way to avoid or resolve complexities associated with shallow and transient processes is to collect closely spaced heat flow data co-located with seismic reflection and swath map data, so that areas of recent mass movement can be avoided, and to verify the consistency of results through a combination of regional and local measurement campaigns. There may be a nearby oceanographic buoy, or long-term temperature loggers can be left on the seafloor in advance to provide a baseline record from months or years prior to heat flow surveys (Hamamoto *et al.* 2005). Bottom water temperature variations tend to be small at water depths ≥2–3 km (Davis *et al.* 2003), but some deep marine environments remain susceptible to

changes in seafloor temperature (e.g., Barker & Lawver 2000; Fukasawa *et al.* 2003).

GLOBAL CONSIDERATIONS

Lithospheric cooling models simulate how the lithosphere cools, contracts, and subsides as it ages. Lithospheric cooling rates are estimated from bathymetry (related to the lithospheric heat content) and heat flow measurements from older seafloor, from which heat transfer is thought to be dominantly conductive. These models comprise a reference against which heat flow observations are compared, providing the basis for quantifying anomalies and calculating the extent of advective plate cooling. The two main types of cooling models (constant thickness plate, thickening half space) make similar predictions for young to middle aged seafloor heat flow as a function of lithospheric age (Parker & Oldenberg 1973; Parsons & Sclater 1977; Davis & Lister 1974; McNutt 1995; Harris & Chapman 2004). Both classes of model predict seafloor heat flow to vary as $C/\sqrt{age}$ initially. The dependence continues to great age for the half space model, whereas there is an asymptotic heat flow value for old seafloor predicted by the plate model. When heat flow is in mW m^{-2} and *age* is in millions of years, the magnitude of the best-fitting value of C is ~475–510, depending on the data and methods used.

The plate model is based on constant plate thickness at all ages, even at spreading centers where new seafloor is created. With time the plate cools until equilibrium is achieved between heating from below and heat loss at the top. In contrast, the half space model is based on the lithosphere having zero thickness at the ridge, then cooling and thickening with age. This model predicts heat flow less (and depths greater) than commonly observed on old seafloor. Some differences between the two models can be reconciled if there are additional inputs of heat into the base of older lithosphere. There has been limited recent discussion about the theoretical basis for lithospheric cooling models, but the fundamental issues and the global extent of hydrothermal cooling of the ocean basins are well-established, heavily documented by observational data, and considered reliable by the vast majority of active practitioners (e.g., Von Herzen *et al.* 2005).

Analysis of the global marine heat flow data set shows that the conductive heat flow from young lithosphere is generally lower than predicted by standard cooling models (Fig. 2A). The heat flow deficit is greatest when the seafloor is young, and extends on average to ~65 Ma. However, there are numerous older seafloor sites that appear to lose some heat advectively, and additional regions of old seafloor where heat may be redistributed locally by vigorous convection within basement, even if there is no net advective heat loss from the plate (Von Herzen 2004).

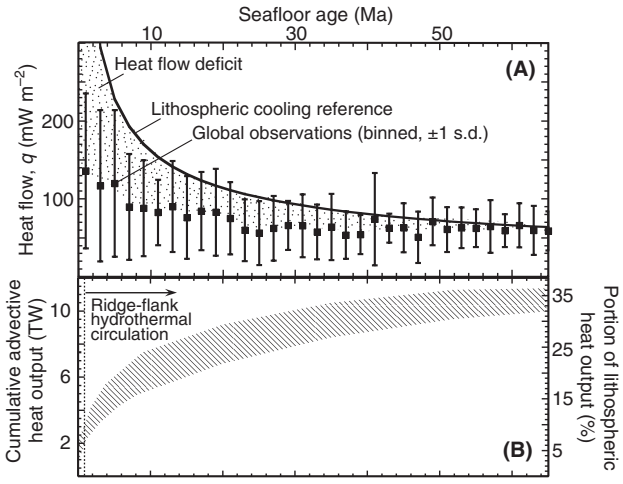

Fig. 2. (A) Schematic comparison between standard lithospheric cooling models (solid curve) and global compilations of oceanic heat flow measurements (solid squares = 2 Ma bin averages, error bars = ±1 SD). The difference between modeled and observed values is the conductive heat flow deficit, generally attributed to advective heat loss. The observed variability of measurements is often attributed to local advective redistribution of heat by vigorous convection in basement. (B) Cumulative global advective heat output, based on integrated difference between lithospheric and observed heat flow values, taking into account the area of seafloor occupied by each age bin. Band indicates a range of values from different studies (Sclater *et al.* 1980; Stein *et al.* 1995; Mottl 2003). Advective heat loss at seafloor spreading centers comprises a fraction of the total advective heat loss, with the majority occurring on ridge flanks.

When the marine heat flow deficit is integrated across the area of the seafloor as a function of age, the global advective heat loss from the ocean crust is ~10 TW, ~25% of Earth's current geothermal heat output, and ~35% of the heat lost through the seafloor by conduction and advection combined (Sclater *et al.* 1980; Stein & Stein 1994; Mottl 2003) (Fig. 2B). Of this advective heat loss, 2–3 TW occurs at or near seafloor spreading centers, and the remaining 7–8 TW occurs on ridge flanks, far from the magmatic influence of lithospheric creation.

The total fluid flux (F) implied by the global advective heat output (Q_{adv}) is calculated as:

$$F = \frac{Q_{adv}}{(\rho c)_f \Delta T} \quad (4)$$

where $(\rho c)_f$ is the heat capacity of hydrothermal fluid, and ΔT is the difference in temperature between oceanic bottom water and hydrothermal discharge. Thus the calculated fluid flux scales linearly with the characteristic temperature of fluid circulation. Field studies of ridge flank areas from which a significant fraction of lithospheric heat loss is advective show that typical basement temperatures are on the order of 5–40°C, which implies that $F = 10^{15}$–10^{16} kg $year^{-1}$ (Stein & Stein 1994; Mottl 2003), a flow rate approaching that of all of rivers and streams into the ocean.

The comparison of thousands of seafloor heat flow observations to well-established models of lithospheric cooling provides a robust estimate of the total amount of water that must flow between the crust and ocean. This information can be combined with highly idealized models to estimate bulk crustal properties on a global or time-dependent basis (e.g., Fisher & Becker 2000). However, the comparison of age-binned data to models tells us little about specific processes or properties at individual field sites. Resolving these characteristics requires application of regional and local models. This is especially important for understanding the variability in heat flow values observed in many surveys, once considered to be noise but now understood to result from fundamental physical processes, as described in the following section.

REGIONAL AND LOCAL CONSIDERATIONS

Regional and local models

Multiple processes can contribute to anomalous seafloor heat flow (Fig. 3). In locations where there is relatively flat seafloor and buried basement relief, conductive refraction tends to increase heat flow immediately above an elevated basement area, because basalt of the upper ocean crust tends to have a thermal conductivity that is greater than that of typical marine sediments (Fig. 3A). Heat flow can be further elevated above a buried basement high if there is vigorous local convection in the shallow crust, making uppermost basement isothermal (Davis *et al.* 1989; Fisher *et al.* 1990). In practice, it can be difficult to distinguish between these two processes based on the general pattern of seafloor heat flow, but modeling can quantify the extent of the necessary thermal conductivity contrast or homogeneity in basement temperatures (Davis *et al.* 1997b).

Recharge of bottom seawater though areas of basement exposure, followed by rapid lateral flow and mixing within the crust, can suppress seafloor heat flow on a regional basis (Fig. 3B). The extent of suppression can be calculated through application of the 'well-mixed aquifer' (WMA) model, a one-dimensional representation of vertical heat flow through a horizontal flow system (Langseth & Herman 1981). The upper oceanic crust is idealized as having a conductive boundary layer (sediments), underlain by an aquifer (shallow basement), within which there is thermally significant lateral transport. Recharge to the aquifer occurs at the temperature of bottom water, and heat is exchanged with the crust during lateral flow. The aquifer is assumed to be well mixed vertically, having a temperature determined by the balance between heat entering from below and leaving through the conductive upper boundary. Key information required to compare observations to predictions based on the WMA model includes: measured seafloor heat flow, the distance from the measurement points to the site of recharge, the thicknesses of the conductive layer and the permeable rock layer through which fluid flows laterally, estimated heat input from below the aquifer (often assumed to be lithospheric), and thermal properties of the sediment and rock/fluid system. The WMA model can be extended to include a second conductive boundary layer below sediments and above permeable basement (e.g., Rosenberg *et al.* 2000).

The influence of basement relief, local convection, and regional advection may be combined if there is outcrop-to-outcrop circulation (Fig. 3C). Seawater entering the crust, circulating laterally, then existing the crust can carry a significant fraction of lithospheric heat if fluid fluxes are sufficiently large, leaving the conductive seafloor heat flow suppressed between recharge and discharge sites (Davis *et al.* 1992; Villinger *et al.* 2002; Fisher *et al.* 2003b). This process can lead to very low heat flow adjacent to areas where hydrothermal recharge occurs, and locally elevated values adjacent to locations where warmed fluids rise rapidly and exit the crust, even when the rate of fluid flow is insufficient to mine heat from the lithosphere regionally (Fisher *et al.* 2003a).

For each of the situations described above, the sediments overlying basement were assumed to act as a conductive boundary layer, with the most vigorous circulation occurring within underlying basement. Most marine sediments have a permeability orders of magnitude less than that of volcanic rocks from the upper oceanic crust (Spinelli *et al.* 2004). Because of this, and because driving forces for hydrothermal circulation are limited, there is little fluid flow through sediments that extracts significant quantities of lithospheric heat. The vast majority of seafloor heat flow measurements indicate conductive conditions within shallow sediments.

Where there is a component of vertical flow through sediments that perturbs the local geothermal gradient, deviations from conductive conditions can be used to estimate the seepage rate. One model used for interpretation of vertical seepage is based on flow through a layer having constant temperature boundaries at the top and bottom (Fig. 3D) (Bredehoeft & Papadopulos 1965). The assumption that upper and lower boundaries have fixed temperatures is most appropriate when the flow through the layer is modest relative to the size of overlying and underlying reservoirs. In the case of seafloor hydrologic systems, this model has been applied most commonly to marine sediments, bounded at the top by the ocean (essentially an infinite sink for heat), and at the base by a large hydrothermal reservoir. The minimum seepage rate necessary for detection of deviations from conductive conditions depends on the thickness of the boundary layer and the depth extent of measurements. For conductive heat flow of 2 W m^{-2} across a layer 20-m thick, a flow rate

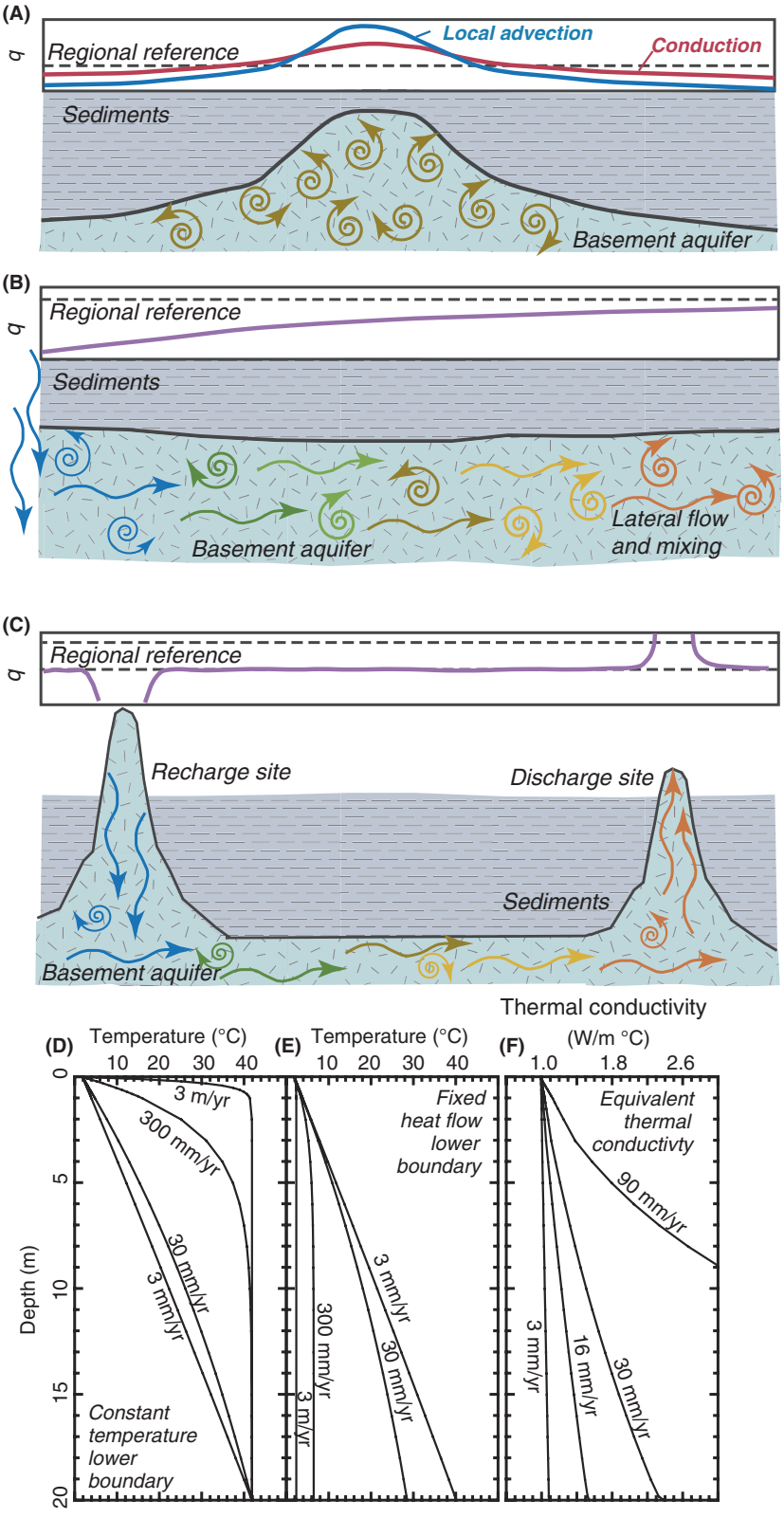

Fig. 3. Illustrations of how regional and local fluid flow can influence seafloor heat. The dashed line labeled ''*regional reference*'' in panels A–C could be lithospheric, or could be a lower or higher value that is typical of regional conditions. (A) Buried basement highs can cause conductive refraction, increasing heat flow through overlying sediments. Vigorous local convection can make the sediment–basement interface isothermal, raising heat flow at the seafloor above the basement high even more, depending on the extent of relief and isothermal conditions. B. Recharge of cold bottom water into the seafloor lowers heat flow in nearby areas, with heat flow rising as fluids in the underlying aquifer flow laterally, mix vertically, and are heated (Langseth & Herman 1981). (C) Outcrop-to-outcrop circulation lowers seafloor heat flow immediately adjacent to areas of local recharge, and raises seafloor heat flow immediately adjacent to areas of hydrothermal discharge. Regional heat flow may be suppressed between outcrops if fluid circulation is sufficiently vigorous and extensive (e.g., Davis *et al.* 1992; Fisher *et al.* 2003b), or regional heat flow may be essentially unaffected by this form of circulation (Hutnak *et al.* 2006). (D) Upward fluid seepage can cause curvature in thermal gradients, with temperatures held constant at the top and bottom of the boundary layer (Bredehoeft & Papadopulos 1965). The extent of curvature depends on the thickness of the layer, background gradient, thermal properties, and fluid flow rate. In this example, the layer is 20 m thick, thermal conductivity is 1 W (m °C)$^{-1}$, background heat flow is 2 W m^{-2}, and fluid flow rates are as indicated. (E) As an alternative, the top of the boundary can be held at constant temperature, and total heat flow through the layer (advective and conductive) can be fixed (Wolery & Sleep 1975). Many geological systems are likely to function somewhere these two end members. (F) Thermal conductivity variations that would mimic the flow rates shown by causing curvature in the conductive thermal gradient based on the Bredehoeft & Papadopulos (1965) model (panel D).

≥30 mm year^{-1} may be required. Heat flow measurements made with shorter probes require greater advective transport in order to be detected.

An alternative application involves a case when the heat input to the base of the sediment layer is limited, rather than being infinite (Fig. 3E) (Wolery & Sleep 1975). In

this case, the conductive gradient is reduced as upward seepage (and heat advection) increases. Conditions in many marine hydrologic systems are likely to be somewhere between these two endmembers. The seafloor boundary condition can reasonably be assumed constant, but the lower boundary condition may be neither constant temperature nor constant heat flow.

In practice, interpretations of thermally significant seepage through sediments should be applied cautiously, because the forces available to drive fluids through marine sediments are limited in many settings, and because systematic changes in thermal conductivity can lead to curvature in thermal gradients under conditions of conductive heat flow (Fig. 3F). Vertical analytical models of coupled fluid-heat flow have been modified to account for lateral flow (e.g., Lu & Ge 1996), but this is rare in shallow sediments, because the sedimented seafloor is usually flat or gently sloped and lateral pressure gradients tend to be small. An exception to this latter generalization is presented in the following section, and subsequent sections show how arrays of heat flow measurements can be used to resolve lateral flow rates in basement.

Multiple scales of fluid circulation: Middle Valley, northern Juan de Fuca Ridge

There are few heat flow studies of active seafloor spreading centers based on measurements of shallow thermal conditions because most such areas are characterized by large regions of basement exposure and limited sediment cover. The most common means for assessing hydrothermal output on young seafloor is through measurement of the heat content of chronic plumes formed by discharge hot, highly altered hydrothermal fluids (Baker & Hammond 1992; Veirs *et al.* 1999). Plume studies have shown that the advective heat output associated with seafloor spreading scales with spreading rate, and that the advective heat output of these areas is generally consistent with crystallization and cooling of the upper 1–2 km of oceanic crust (Baker 2007).

There are three very young (essentially 0–0.1 Ma) sites where seafloor heat flow surveys have been conducted: Guaymas Basin in the Gulf of California, Escanaba Trough on the Gorda Ridge, and Middle Valley at the northern end of the Juan de Fuca Ridge (Lonsdale & Becker 1985; Abbott *et al.* 1986; Davis & Villinger 1992). All three are sedimented spreading centers, located adjacent to continental areas where thick sediments trap heat within the subsurface, compressing thermal and chemical gradients near the seafloor, focusing hydrothermal recharge and discharge, and allowing thermal and fluid flow regimes to be characterized through coring, drilling, and heat flow surveys (Davis & Villinger 1992; Gieskes *et al.* 1982; Kastner 1982; Stein & Fisher 2001; Wheat & Fisher 2007). Studies from these areas provide unique insights on coupled fluid–thermal processes within very young seafloor.

Middle Valley (Figs 4A and 5A) is bordered by ridge-parallel, high-angle normal faults and filled with Pleistocene turbidites and hemipelagic clay deposited when sea level was lower and terrigeneous sediments were transported down the continental slope and into Cascadia Basin (Davis & Villinger 1992). As at other sedimented spreading centers, basaltic magma rises from depth and intrudes laterally as sills within thick sediments rather than erupting at the seafloor. Upper lithologic 'basement' in this setting comprises alternating sills and indurated sediments having bulk permeability much greater than that of overlying sediments (Becker *et al.* 1994; Fisher *et al.* 1994; Langseth & Becker 1994). This sediment–sill sequence hosts vigorous hydrothermal circulation that leads to essentially isothermal (280°C) conditions in uppermost basement (Davis & Fisher 1994; Davis & Villinger 1992; Davis & Wang 1994). Although Middle Valley remains tectonically and hydrothermally active, it appears that the primary focus of seafloor spreading is currently shifting to the adjacent West Valley.

The total heat flux from a 260 km^2 area of Middle Valley suggests heat output at a spatial rate of 16 MW km^{-1} of ridge (Stein & Fisher 2001), a value consistent with estimated heat output from other (unsedimented) parts of

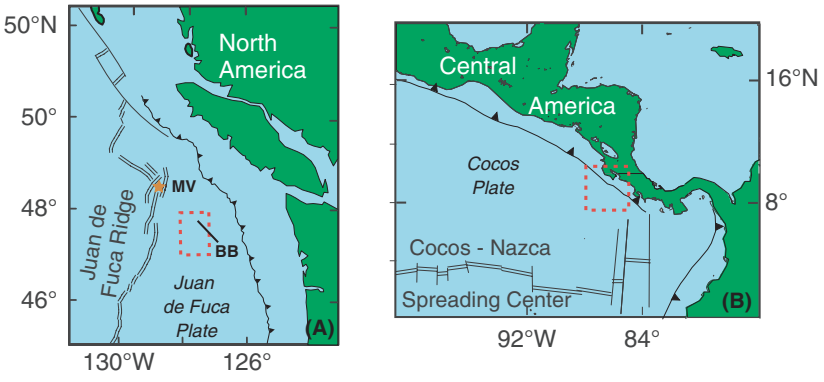

Fig. 4. Regional index maps showing locations of field areas discussed in this paper. (A) Northeastern Pacific Ocean. MV = Middle Valley. BB = Baby Bare outcrop. Dashed red box is area of Fig. 6A. (B) Eastern Equatorial Pacific Ocean. Dashed red box is area of Fig. 7.

the Juan de Fuca Ridge (Baker 2007). But in contrast to more normal seafloor spreading centers, conductive and advective heat outputs from Middle Valley are about equal in magnitude. Bare rock spreading centers are thought to release the vast majority of their heat advectively.

The Dead Dog vent field within Middle Valley has been explored with numerous instruments, including a side-scan survey that defined the area of active venting (AAV) based on high acoustic backscatter (Davis & Villinger 1992) (Fig. 5B). Within the AAV there are ~20 vents discharging hydrothermal fluid at temperatures up to 280°C. A scientific drill hole placed near the center of this AAV cored extrusive basaltic rocks below ~260 of turbidites and hemipelagic clay. Repeated heat flow surveys (including data from multipenetration probes and outriggers probes attached to core barrels) show that the highest values are found immediately adjacent to active vents (Fig. 5B). Interestingly, some of the lowest heat flow values were also measured close to active vents.

The mean heat flow of ~10 W m^{-2} within the Dead Dog AAV has been interpreted to result from formation of a diagenetic and hydrologic cap above a shallow hydrothermal reservoir (Davis & Villinger 1992; Davis & Fisher 1994; Stein *et al.* 1998; Stein & Fisher 2001). Fluid convects vigorously below the cap, helping to maintain isothermal conditions near 280°C at ~30 m below the seafloor. There may be additional focusing of conductive heat flow because of refraction related to the buried basement edifice and shallow sulfide deposits, both of which have greater thermal conductivity than typical marine sediments (Fig. 3A).

The scattering of heat flow values both above and below the mean of ~10 W m^{-2} within the AAV can be explained by proximity to active vents, as demonstrated with coupled numerical modeling (Fig. 5C and D). The vents act as conductive heat sources as hydrothermal fluid rises to the seafloor, warming shallow sediments around the vents, and elevating heat flow to values ≥50 W m^{-2}. In addition, local recharge associated with secondary convection can suppress heat flow to <1 W m^{-2} close to vents. This secondary convection cannot be a significant mechanism for recharging the main hydrothermal system because fluid samples collected from the vents show no indication of mixing between hydrothermal fluid and ambient seawater, and there is little evidence for water–sediment interaction prior to fluid discharge (Butterfield *et al.* 1994). Instead, it is likely that recharge of fluids supporting high-temperature discharge in Middle Valley occurs mainly along faults and

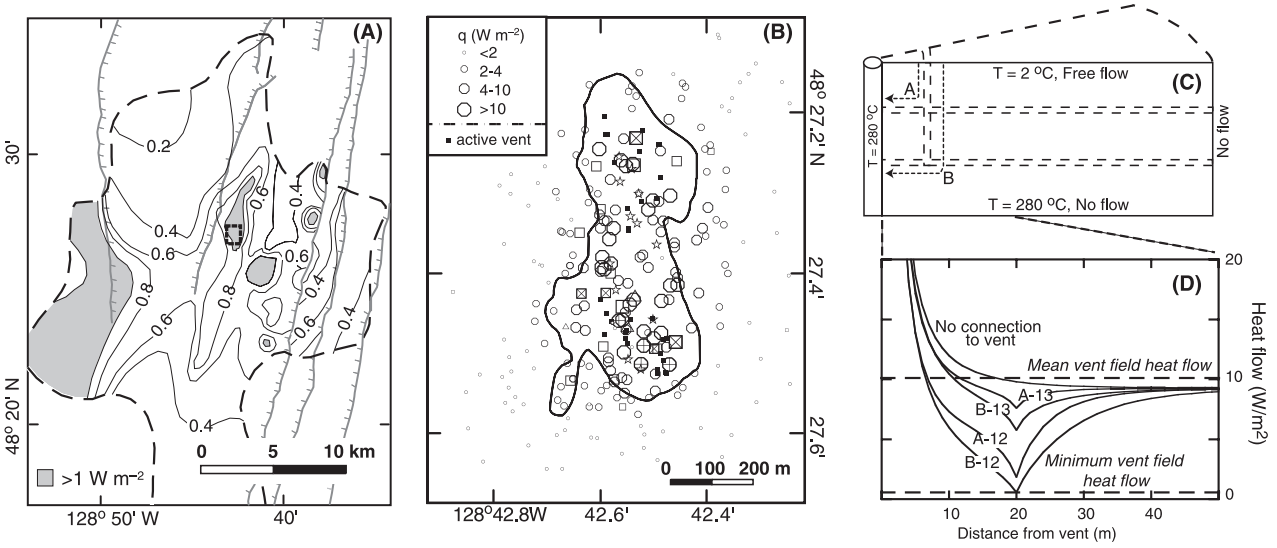

Fig. 5. Diagrams showing data and model results from Middle Valley, northern Juan de Fuca Ridge. Figures modified from Davis & Villinger (1992) and Stein & Fisher (2001). (A) Regional view of Middle Valley, showing valley bounding normal faults (thin lines with ticks) and area of the most complete coverage of seafloor heat flow measurements (within thicker dashed line). Contours show typical heat flow values (units of W m^{-2}), and grey areas show where heat flow is ≥1 W m^{-2}. Dotted box shows area of Fig. 5B. (B) Area of active venting (AAV) including the Dead Dog vent field. Edge of AAV identified by side scan sonar surveys (Davis & Villinger 1992). Open circles indicate location and magnitude of heat flow values, as labeled. Solid squares are individual hydrothermal vents. Crosses indicate at least one thermistor exceeded maximum temperature range of instrument (40°C). Stars indicate locations where the heat flow probe fell over without penetrating. (C) Schematic of radial cross-section used in simulations of secondary circulation around a hydrothermal vent. Horizontal (10 and 20 mbsf) and vertical (20 m from vent) 1-m thick channels were used in some simulations, labeled to show flow paths A and B, respectively. (D) Surface heat flow versus distance from vent for simulations with secondary hydrothermal convection. Background heat flow is 10 W m^{-2}. Conductive case is shown for reference with no connection to vent. Cases A and B have a shallower and deeper connection to the hydrothermal vent, respectively, and each is run with connection permeability of 10^{-12} m^2 and 10^{-13} m^2 as shown. The deeper the horizontal layer and the higher its permeability, the more efficient the local heat flow reduction associated with secondary convection.

other isolated conduits along the edges of the valley (Davis & Villinger 1992; Stein & Fisher 2001; Wheat & Fisher 2007). In summary, heat flow and other data from Middle Valley resolve multiple scales of fluid circulation, delineate conditions and the depth to the top of a hydrothermal reservoir, and help to define the regional geometry of fluid flow, including the importance of basement outcrops in guiding hydrothermal recharge. The extent to which these results can be applied to more normal (bare rock) seafloor spreading centers remains to be determined.

FLUID FLOW THROUGH OUTCROPS: EASTERN FLANK OF THE JUAN DE FUCA RIDGE

Numerous physical and chemical surveys have been completed on 0.7–3.6 Ma seafloor on the eastern flank of the Juan de Fuca Ridge (Davis *et al.* 1992, 1999; Wheat & Mottl 1994, 2000; Thomson *et al.* 1995; Elderfield *et al.* 1999; Fisher *et al.* 2003a; Hutnak *et al.* 2006; Wheat *et al.* 2004). Oceanic basement rocks in this area were formed at the unsedimented Endeavour segment of the Juan de Fuca Ridge, but were subsequently covered at a young age by hemipelagic clay and turbidites. Basement rocks remain exposed close to the active spreading center and where seamounts and other basement outcrops are found up to 100 km to the east. Three basement outcrops were identified initially in this area: Papa Bare, Mama Bare, and Baby Bare (Fig. 6A) (Davis *et al.* 1992; Thomson *et al.* 1995; Mottl *et al.* 1998). These outcrops are volcanic cones created off-axis on top of preexisting abyssal hill topography.

Baby Bare outcrop is the smallest and most extensively surveyed of the three outcrops, rising 70 m above the surrounding seafloor and covering an area of 0.5 km^2. Although the elevated area of this feature is small, the buried Baby Bare edifice rises ~600 m above the top of regional volcanic crustal rocks. Analysis of altered rocks, sediment pore fluids, and shallow thermal gradients on Baby Bare outcrop indicate that this feature discharges 5–20 L s^{-1} of hydrothermal fluid (Thomson *et al.* 1995; Mottl *et al.* 1998; Becker *et al.* 2000; Wheat *et al.* 2004).

Mama and Papa Bare outcrops (Fig. 6A) are also sites of ridge-flank hydrothermal discharge, although these features have not been surveyed as completely as Baby Bare. Mama Bare outcrop is located 14 km northeast of Baby Bare outcrop on the same basement ridge, covers an area of 0.9 km^2, and rises 140 m above the surrounding seafloor. Papa Bare outcrop is located on an adjacent buried

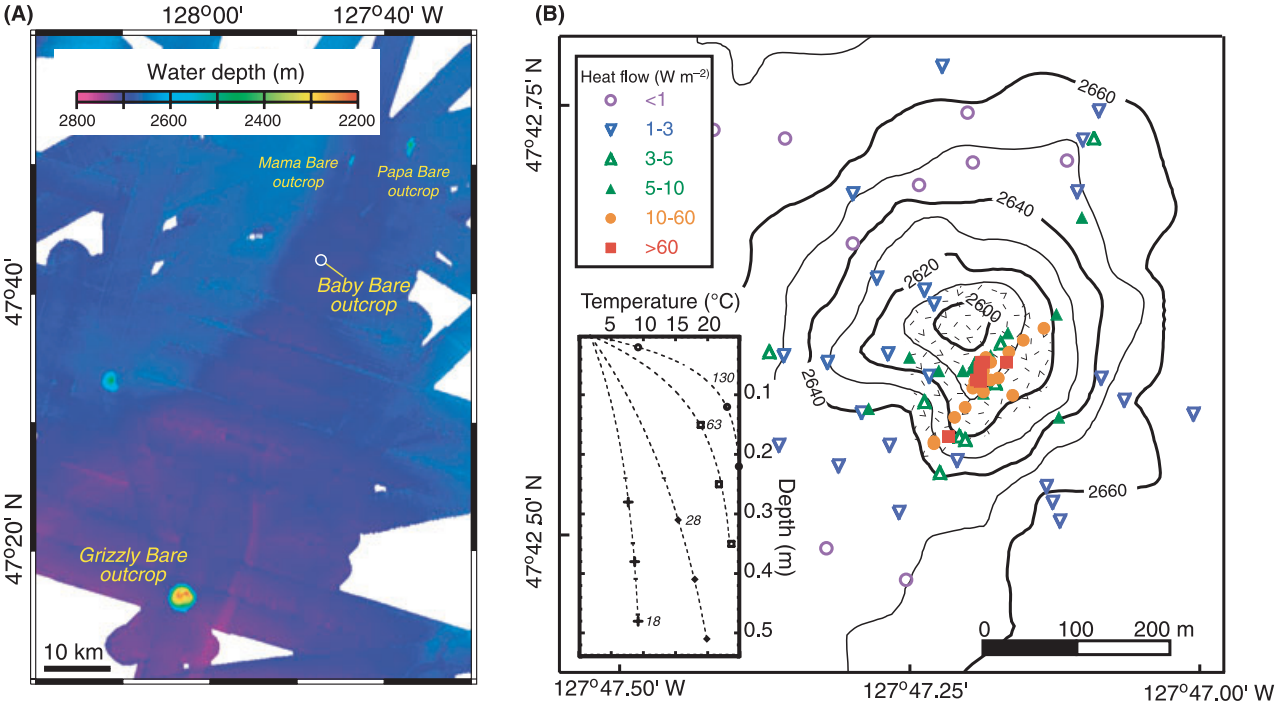

Fig. 6. Maps of field area on the eastern flank of the Juan de Fuca Ridge (index map shown in Fig. 4A). (A) Regional map showing locations of basement outcrops on 3.5–3.6 Ma seafloor (modified from Hutnak *et al.* 2006). Baby Bare, Mama Bare, and Papa Bare outcrops are sites of hydrothermal discharge, whereas Grizzly Bare is a site of hydrothermal recharge (Fisher *et al.* 2003a). (B) Fine scale topographic map of Baby Bare outcrop, with locations of heat flow measurements made with the submersible, *Alvin* (Wheat *et al.* 2004). Highest heat flow values are associated with a normal fault on the eastern side of the outcrop. Several of these heat flow values are based on curved gradients, as shown in the inset diagram. Numbers in the inset indicate apparent seepage rates, in m $year^{-1}$, based on application of the model shown in Fig. 3D.

basement ridge to the east, covers an area of 2.6 km^2, and rises 240 m above the surrounding seafloor. As with Baby Bare outcrop, most of the Papa and Mama Bare edifices are buried by thick sediments. Interestingly, no hydrothermal recharge sites have been identified on any of these three features.

Consideration of ridge-flank hydrothermal driving forces, basement fluid chemistry, and sediment properties precludes recharge of Baby Bare outcrop through the seafloor surrounding the basement edifice; instead, fluids recharge through Grizzly Bare outcrop 52 km to the south (Fig. 6A) (Fisher *et al.* 2003a). Grizzly Bare outcrop is conical in shape, 3.5 km in diameter, and rises 450 m above the surrounding seafloor. The consistency of their alignment and strike with regional basement topography (Wilson 1993; Zühlsdorff *et al.* 2005) suggests that the Grizzly, Baby, and Mama Bare outcrops may have formed along the same buried abyssal hill. Fluid flow in basement between Grizzly Bare and Baby Bare outcrops may be facilitated by enhanced permeability in a direction parallel to the abyssal hill topography (Fisher *et al.* 2003a, 2008; Wheat *et al.* 2000). Grizzly Bare outcrop was identified as a site of hydrothermal recharge based initially on patterns of seafloor heat flow immediately adjacent to the edifice. Seafloor heat flow is depressed within a few kilometers of the edge of basement exposure along several transects of measurements (Fisher *et al.* 2003a; Hutnak *et al.* 2006). Seismic reflection data allow determination of sediment thicknesses at heat flow measurement locations, and downward continuation of thermal data through the sediment shows that isotherms are swept downwards by cold, recharging fluid in the sediments and shallow basement adjacent to the outcrop edge. In contrast, warm fluid discharge from Baby Bare outcrop causes extremely high seafloor heat flow, and an upward sweeping of isotherms, adjacent to the area of exposed basement (Davis *et al.* 1992; Fisher *et al.* 2003a).

Baby Bare outcrop was surveyed repeatedly using the submersible *Alvin*, including high-resolution bathymetric mapping, geological and pore fluid sampling, and heat flow measurements (Wheat *et al.* 2004) (Fig. 6B). The *Alvin* heat flow probes used on these surveys were ~0.60 m long and contained three or five thermistors. A constant thermal conductivity of 0.89 W $(m\ °C)^{-1}$ was assumed for all Baby Bare heat flow measurements (Wheat *et al.* 2004), based on *in situ* and needle probe measurements of material recovered nearby during subsequent surveys (Fisher *et al.* 2003a; Hutnak *et al.* 2006). Most heat flow values measured on Baby Bare outcrop were >1 W m^{-2}, well above values measured on the adjacent flat seafloor, and the highest Baby Bare values were >100 W m^{-2}. There is an area of elevated heat flow aligned along a linear trend on the southwest side of the outcrop, adjacent to a normal fault scarp near the outcrop summit (Fig. 6B). Sediment thickness is not well mapped across Baby Bare outcrop because of irregular topography, but the depth to the 64°C isotherm (consistent with regional basement temperatures and fluid chemistry) is generally ≤50 m (Davis *et al.* 1992; Elderfield *et al.* 1999; Hutnak *et al.* 2006; Wheat & Fisher 2007).

Several thermal profiles from Baby Bare outcrop display significant curvature with depth. These thermal profiles were interpreted to indicate fluid flow, through application of the Bredehoeft & Papadopulos (1965) model (Fig. 3D), only if curvature could not be accounted for by reasonable variations in thermal conductivity, and only if the apparent seepage rate exceeded 6.5 m $year^{-1}$ (Fig. 6B, inset, Wheat *et al.* 2004). Other profiles, indicating apparently conductive thermal conditions, were evaluated based on nearby geochemical data from push cores. Geochemical data were fit to an advection–diffusion model similar to that used for assessing curvature in thermal data. But because chemical diffusivity for solutes is about three orders of magnitude smaller than thermal diffusivity, chemical data are much more sensitive to fluid flow. Chemical data were used to estimate seepage rates between 0.005 and 2 m $year^{-1}$, above which chemical concentrations are essentially constant with depth in the upper 0.5 m of sediment. Total heat flow values were calculated as the sum of conductive and advective components (Wheat *et al.* 2004).

Thermal and chemical data were combined to estimate point and total seepage rates, and integrated heat output, from Baby Bare outcrop. These data suggest heat output of ~2 MW for Baby Bare and the immediately surrounding seafloor, a value similar to that estimated in earlier seafloor studies (Mottl *et al.* 1998), and at the lower end of estimates made from thermal anomalies in the overlying water column (Thomson *et al.* 1995). Estimated Baby Bare heat output is about the same as that from a single high-temperature (350°C) hydrothermal vent. The mean heat flow from Baby Bare outcrop is an order of magnitude greater than that estimated from lithospheric cooling models for 3.5 Ma seafloor like that upon which Baby Bare is located. Although there are small areas on Baby Bare outcrop where shimmering water can be seen rising from the seafloor, the thin drape of sediment overlying much of the basement edifice functions effectively as a thermal boundary layer, with vigorous convection in the underlying basement redistributing heat laterally and enhancing the rate of conduction through the top of the edifice. Advective heat loss from Baby Bare outcrop is limited, and the present day circulation system has virtually no influence on regional heat flow (Davis *et al.* 1999; Hutnak *et al.* 2006), although it is likely that advective heat loss was considerably greater in the past, before many other outcrops were covered by thick, low-permeability sediments (Hutnak & Fisher 2007).

Massive fluid fluxes resolved with thermal data: Eastern Cocos Plate

The 18–24 Ma seafloor of the Cocos Plate offshore the Nicoya Peninsula, Costa Rica (Fig. 4B), comprises a northern region formed at the East Pacific Rise (EPR), and a southern region formed at the Cocos-Nazca Spreading Center (CNS) (Fig. 7) (Meschede *et al.* 1998; Ranero & von Huene 2000; von Huene *et al.* 2000; Barckhausen *et al.* 2001). The boundary between EPR- and CNS-generated seafloor is a combination of a triple junction trace and a fracture zone trace, collectively comprising a 'plate suture.' Pre-2000 studies in this area revealed variable thermal conditions (e.g., Langseth & Silver 1996; Vacquier *et al.* 1967; Von Herzen & Uyeda 1963), but the spatial distribution of warmer and cooler seafloor was incomplete, and the extent and nature of hydrothermal activity was unclear. Later surveys included swath-mapping to identify basement outcrops, and multi-channel seismic reflection data to delineate regional tectonic features, sediment thickness, and basement relief (Fisher *et al.* 2003b; Hutnak *et al.* 2007). Multipenetration heat flow data were co-located on seismic reflection profiles to assess heat transport and determine upper basement temperatures; additional heat flow measurements were made with autonomous temperature probes attached to core barrels (Pfender & Villinger 2002; Hutnak *et al.* 2007).

Heat flow surveys documented a thermal transition between warm and cool areas of the Cocos Plate (Fisher *et al.* 2003b; Hutnak *et al.* 2007) (Fig. 7). The mean heat flow through CNS- and EPR-generated seafloor on the warm part of the plate is consistent with lithospheric thermal reference models, 95–120 mW m^{-2} (Parsons & Sclater 1977; Stein & Stein 1994). In contrast, the seafloor heat flow through EPR-generated seafloor northwest of the thermal transition is typically 10–40 mW m^{-2}, just 10–40% of lithospheric values. The thermal transition between warm and cool areas of the plate is only a few kilometers wide (Fig. 8), consistent with advective heat extraction from the shallow crust on the cool side of the plate (Fisher *et al.* 2003b; Hutnak *et al.* 2007). The thermal transition coincides with the plate suture near where the Cocos Plate begins to subduct in the Middle America Trench. But through most of the survey area, the boundary between warmer and cooler parts of the plate is spatially associated with the occurrence of seamounts and other basement outcrops that penetrate regionally extensive sediments (Fig. 7).

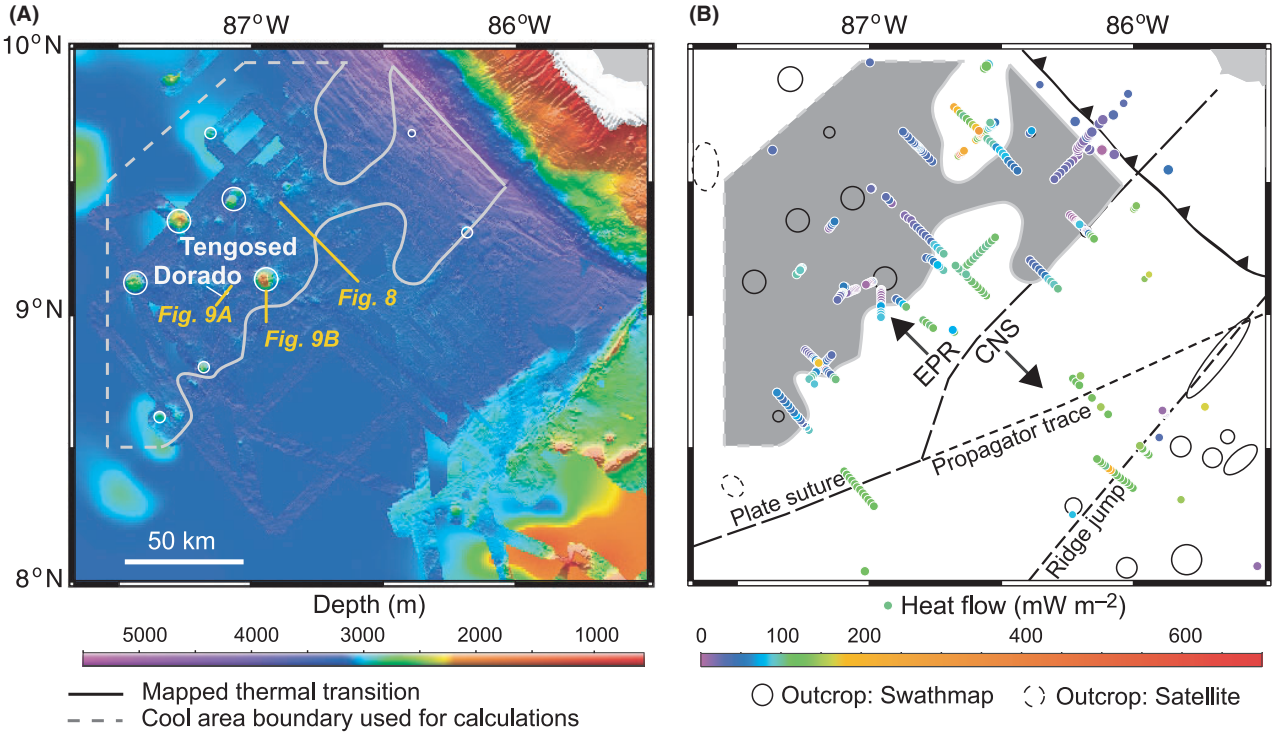

Fig. 7. A. Bathymetric map of field area on 18–24 Ma seafloor of the Cocos Plate, eastern Pacific Ocean (index map shown in Fig. 4B) (modified from Hutnak *et al.* 2008). Dorado outcrop is a site of hydrothermal discharge, whereas Tengosed Seamount is a site of hydrothermal recharge. Gray line demarcates thermal boundary between cooler and warmer parts of the plate. (B) Major tectonic features and results of heat flow surveys. Gray area is cool part of Cocos Plate. Black circles and ovals are seamounts and other basement outcrops apparent on satellite and swath data. EPR = East Pacific Rise. CNS = Cocos-Nazca Spreading Center.

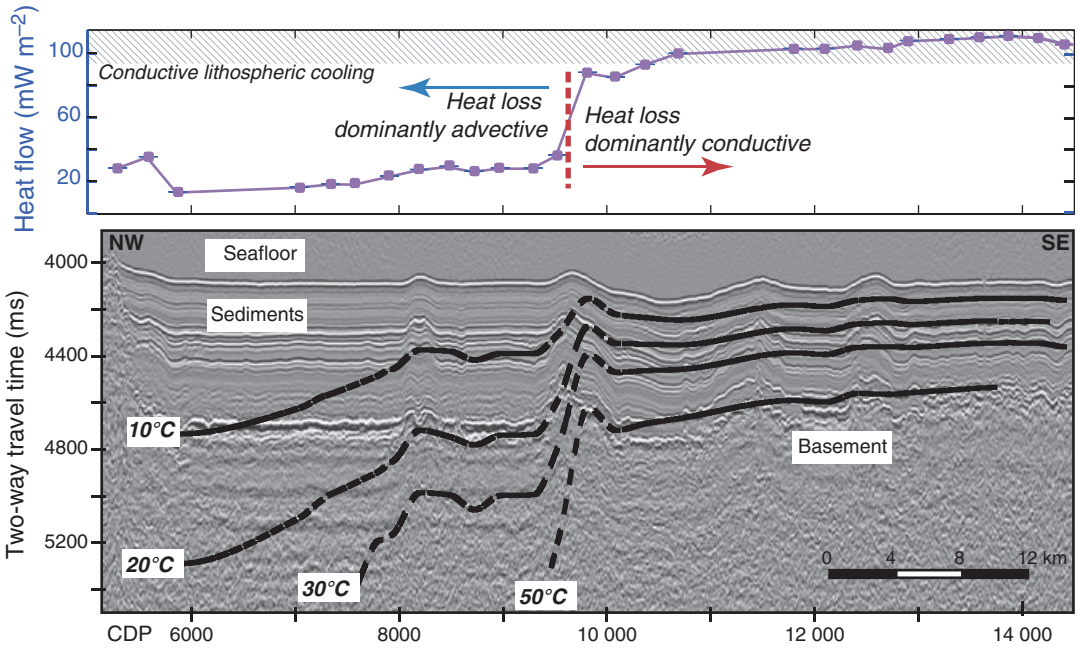

Fig. 8. Co-located heat flow and seismic data that cross the thermal transition between cool and warm parts of the Cocos Plate (location shown in Fig. 7A). Horizontal axis is common depth point (CDP) of the seismic survey. Diagonal band shows range of lithospheric values predicted by standard models for seafloor of this age. Transition between cool and warm parts of the plate occurs across ~2 km, indicating an abrupt change in mechanisms of heat transport in the shallow crust, with vigorous hydrothermal cooling on the northwest side of the transition, and conductive (lithospheric) conditions on the southeast side (Fisher *et al.* 2003b). Isotherms superimposed on the seismic section were calculated by downward continuing heat flow measurements (Hutnak *et al.* 2007).

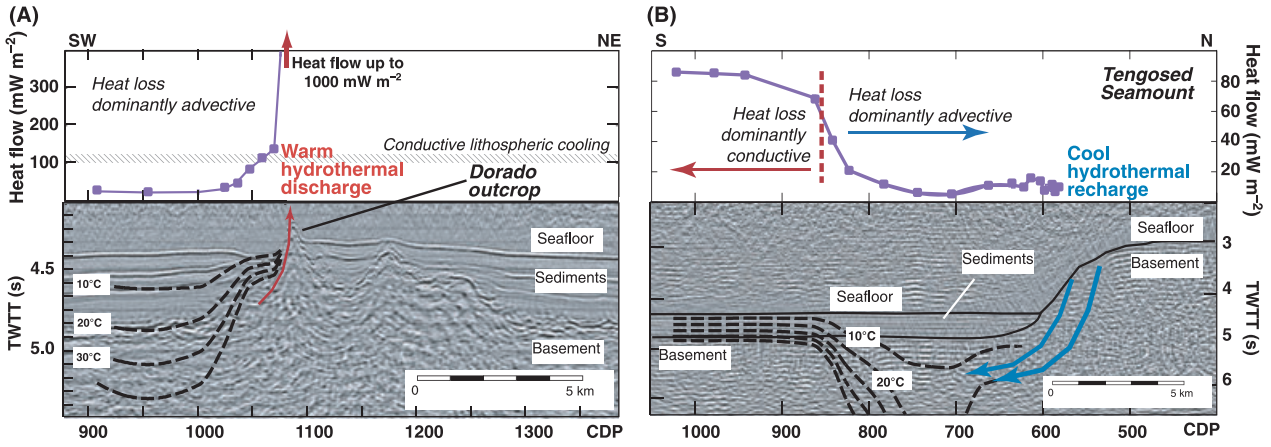

Fig. 9. (A) Seismic and heat flow data near and across Dorado outcrop (location shown in Fig. 7A). Basement rises to penetrate 400–500 m of regionally continuous sediment, and is exposed across a small area of seafloor. Isotherms (black lines) created by downward continuation of heat flow data. Heat flow rises abruptly near the edge of the edifice, but basement temperatures are nearly isothermal at 10–20°C beyond several kilometers from the outcrop. (B) Seismic and heat flow data adjacent to Tengosed Seamount, 20 km east of Dorado (location shown in Fig. 7A). Note differences in vertical scale relative to panel A. Tengosed Seamount is a large edifice rising >1 km above the seafloor, 2 km above regional basement. The upper crust here is chilled below thick sediments by cold bottom water that recharges through exposed basement. Heat flow (and basement temperatures) rise ~10 km south of the outcrop, after passing through the regional thermal transition (dashed red line).

Heat flow and seismic surveys oriented radially away from outcrops indicate that some allow hydrothermal recharge whereas others allow hydrothermal discharge (Hutnak *et al.* 2007, 2008), a pattern similar to that seen on younger seafloor east of the Juan de Fuca Ridge (Davis *et al.* 1992; Fisher *et al.* 2003a; Hutnak *et al.* 2006). Seismic and heat flow data across Tengosed Seamount and Dorado ourcrop, areas of basement exposure separated by 20 km, illustrate characteristic features of this circulation pattern (Figs 7 and 9). Cold fluid recharge is indicated by

a decrease in seafloor heat flow and a downward sweeping of isotherms where sediment thins in proximity to an outcrop. In contrast, warm fluid discharge results in locally elevated seafloor heat flow, and an upward sweeping of isotherms adjacent to an area of exposed basement. In the latter case, the temperature of the sediment–basement contact often remains nearly isothermal as the contact shallows towards the seafloor.

Regional advective power and fluid fluxes from the cold part of the Cocos Plate were quantified using the conductive heat flow deficit (Hutnak *et al.* 2008). There is a 14,500 km^2 area of cool lithosphere on the EPR side of the Cocos Plate. The mean heat flow in this area, away from the local conductive influence basement outcrops and buried ridges, is 29 ± 13 mW m^{-2} (±1 SD), comprising a regional power deficit of 0.8–1.4 GW. Heat flow profiles adjacent to five of the ten mapped basement outcrops in this area indicate recharge through two, discharge through one (Dorado outcrop), one that both recharges and discharges, and one that shows evidence for neither recharge nor discharge (Hutnak *et al.* 2008).

The mean advective power output of individual discharging outcrops on cooler TicoFlux seafloor is 200–350 MW, a range similar to that determined from plume and point studies of high-temperature vent fields on the southern Cleft segment of the Juan de Fuca Ridge (JdFR) and 21°N on the EPR (at the low end) and the Endeavour Main Field on the JdFR and 9°50'N on the EPR (at the high end) (Baker 2007). But in contrast to these ridge-crest systems, the enormous advection of heat from a few outcrops on the Cocos Plate is conveyed by fluids having temperatures only 5–40°C warmer than bottom water (Hutnak *et al.* 2008). Thermal data from the cool side of the Cocos Plate indicate 4–80 × 10^3 L s^{-1} of fluid enters and exits the seafloor in this area. If this fluid flow were distributed across the discharging outcrops, consistent with interpretations from the heat flow surveys, then each discharging outcrop vents 1–20 × 10^3 L s^{-1} of cool hydrothermal fluid (Hutnak *et al.* 2008).

SUMMARY, LESSONS LEARNED, AND PROSPECTS FOR FUTURE WORK

Marine heat flow measurements have helped to quantify fluid flow patterns and rates within the seafloor for more than 30 years. Even before the discovery of seafloor hydrothermal vents, researchers used variations in oceanic heat flow to quantify the extent and nature of hydrogeologic processes in the deep sea. Heat flow data are most useful for this purpose when they are carefully navigated and co-located with reflection seismic and mapping data, so that thermal measurements can be placed in a broader context. It is also helpful to combine thermal studies with coring and chemical analyses, and to obtain high-resolution images or direct observations of seafloor conditions, so that the significance of small-scale variations in heat output can be understood. This has become the standard mode of operation for modern seafloor heat flow studies.

Although the studies described in this review were completed in different hydrogeologic settings, they share several common themes. Marine sediments generally function as a conductive boundary layer separating the volcanic crustal aquifer from the overlying ocean. This is a benefit for using seafloor heat flow to map fluid flow, because the (sedimentary) conductive boundary layer provides a relatively continuous medium in which measurements can be made, and across which thermal conditions can be determined. There may be thermally significant fluid flow through marine sediments in some locations, but demonstrating this requires that curvature in thermal gradients cannot be explained by reasonable differences in thermal conductivity.

In fact, thermally significant fluid seepage through seafloor sediments is relatively rare, being restricted to locations where sediments are thin or unusually permeable, or where driving forces are unusually high. Patterns of conductive heat flow through marine sediments can be used to map out directions and assess rates of fluid circulation within the underlying crust, and are particularly helpful in identifying locations of fluid recharge and discharge near where basement rocks are exposed. Seafloor heat flow measurements are less helpful in resolving the nature of fluid pathways at depth within the crust, but this issue is being addressed to some extent with analysis of core samples and single-hole and multi-hole measurements and experiments (e.g., Becker *et al.* 1983; Anderson *et al.* 1985; Bartetzko *et al.* 2001; Alt & Teagle 2003; Becker & Davis 2005; Fisher *et al.* 2008).

The continued interest in using heat as a tracer to map fluid flow; more common acquisition of complementary data such as high-resolution digital maps and seismic reflection profiles; and the development of new instruments, analytical techniques, and models, is bringing new attention and new practitioners to the field. Most of the seafloor remains poorly mapped and virtually unexplored with regard to thermal and hydrogeologic conditions. Seafloor heat flow remains an important tool for researchers studying coupled fluid, thermal, chemical, tectonic, magmatic, and biological processes. Heat flow measurements are particularly helpful for quantifying local and regional heat and fluid flow rates, and for mapping the plumbing of subseafloor hydrogeologic systems.

ACKNOWLEDGMENTS

This work was supported by National Science Foundation grants OCE-0727952 and OCE-0849354 (ATF) and grants OCE-0637120 and OCE-0849341 (RNH). The authors appreciate thoughtful comments by two

external reviewers that improved the clarity and focus of this paper.

REFERENCES

Abbott DH, Morton JL, Holmes ML (1986) Heat flow measurements on a hydrothermally active, slow spreading ridge: the Escanaba Trough. *Geophysical Research Letters*, **13**, 678–80.

Alt JC, Teagle DAH (2003) Hydrothermal alteration of upper oceanic crust formed at a fast spreading ridge: mineral, chemical, and isotopic evidence from ODP Site 801. *Chemical Geology*, **201**, 191–211.

Anderson MP (2005) Heat as a ground water tracer. *Ground Water*, **43**, 1–18.

Anderson RN, Hobart MA (1976) The relationship between heat flow, sediment thickness, and age in the eastern Pacific. *Journal of Geophysical Research*, **81**, 2968–89.

Anderson RN, Zoback MD, Hickman SH, Newmark RL (1985) Permeability versus depth in the upper oceanic crust: in-situ measurements in DSDP Hole 504B, eastern equatorial Pacific. *Journal of Geophysical Research*, **90**, 3659–69.

Baker ET (2007) Hydrothermal cooling of midocean ridge axes: Do measured and modeled heat fluxes agree. *Earth and Planetary Science Letters*, **263**, 140–50.

Baker ET, Hammond SR (1992) Hydrothermal venting and the apparent magmatic budget of the juan de fuca ridge. *Journal of Geophysical Research*, **97**, 3443–56.

Baker ET, Massoth GJ, Feely RA, Embly RW, Thomson RE, Burd BJ (1995) Hydrothermal event plumes from the CoAxial seafloor eruption site, Juan de Fuca Ridge. *Geophysical Research Letters*, **22**, 147–50.

Barckhausen U, Renaro C, von Huene R, Cande SC, Roeser HA (2001) Revised tectonic boundaries in the Cocos Plate off Costa Rica: implications for the segmentation of the convergent margin and for plate tectonic models. *Journal of Geophysical Research*, **106**, 19.

Barker P, Lawver L (2000) Anomalous temperatures in central Scotia Sea sediments – bottom water variation or pore water circulation in old crust. *Geophysical Research Letters*, **27**, 13–6.

Bartetzko A, Pezard P, Goldberg D, Sun Y-F, Becker K (2001) Volcanic stratigraphy of DSDP/ODP Hole 395A: an interpretation using well-logging data. *Marine Geophysical Researches*, **22**, 111–27.

Becker K, Davis EE (2005) A review of CORK designs and operations during the Ocean Drilling Program. In: *Proc. IODP, Expedition Reports* (eds Fisher AT, Urabe T, Klaus A) College Station, TX, *Integrated Ocean Drilling Program*, **301**, doi:10.2204/iodp.proc.2301.2104.

Becker K, Langseth M, Von Herzen RP, Anderson R (1983) Deep crustal geothermal measurements, Hole 504B, Costa Rica Rift. *Journal of Geophysical Research*, **88**, 3447–57.

Becker K, Morin RH, Davis EE (1994) Permeabilities in the Middle Valley hydrothermal system measured with packer and flowmeter experiments. In: *Proc. ODP, Sci. Res.* (eds Davis EE, Mottl MJ, Fisher AT, Slack JF) College Station, TX, *Ocean Drilling Program*, **139**, 613–26.

Becker NC, Wheat CG, Mottl MJ, Karsten JL, Davis EE (2000) A geological and geophysical investigation of Baby Bare, locus of a ridge flank hydrothermal system in the Cascadia Basin. *Journal of Geophysical Research*, **105**, 23, 557–568.

Bredehoeft JD, Papadopulos IS (1965) Rates of vertical groundwater movement estimated from the earth's thermal profile. *Water Resources Research*, **1**, 325–8.

Bullard EC (1939) Heat flow in South Africa. *Proceedings of the Royal Society of London, Series A.*, **173**, 474–502.

Bullard EC (1954) The flow of heat through the floor of the Atlantic Ocean. *Proceedings of the Royal Society of London, Series A*, **222**, 408–29.

Bullard EC, Maxwell AE (1956) Heat flow through the deep sea floor. *Advances in Geophysics*, **222**, 408–29.

Burow KR, Constantz J, Fujii R (2005) Heat as a tracer to estimate dissolved organic carbon flux from a restored wetland. *Ground Water*, **43**, 545–56.

Butterfield DA, McDuff RE, Franklin J, Wheat CG (1994) Geochemistry of hydrothermal vent fluids from Middle Valley, Juan de Fuca Ridge. In: *Proc. ODP, Sci. Res.* (eds Davis EE, Mottl MJ, Fisher AT, Slack JF) College Station, TX, *Ocean Drilling Program*, **139**, 395–410.

Constantz J, Stonestrom D, Stewart AE, Niswonger R, Smith TR (2001) Analysis of streambed temperatures in ephemeral channels to determine streamflow frequency and duration. *Water Resources Research*, **37**, 317–28.

Davis EE (1988) Oceanic heat-flow density. In: *Handbook of Terrestrial Heat-Flow Density Determination* (eds Haenel R, Rybach L, Stegena L), pp. 223–60. Kluwer, Amsterdam.

Davis EE, Becker K (1994) Formation temperatures and pressures in a sedimented rift hydrothermal system: 10 months of CORK observations, Holes 857D and 858G. In: *Proc. ODP, Sci. Res.* (eds Davis EE, Mottl MJ, Fisher AT, Slack JF) College Station, TX, *Ocean Drilling Program*, **139**, 649–66.

Davis EE, Becker K (2002) Observations of natural-state fluid pressures and temperatures in young oceanic crust and inferences regarding hydrothermal circulation. *Earth and Planetary Science Letters*, **204**, 231–48.

Davis EE, Fisher AT (1994) On the nature and consequences of hydrothermal circulation in the Middle Valley sedimented rift: inferences from geophysical and geochemical observations, Leg 139. In: *Proc. ODP, Sci. Res.* (eds Davis EE, Mottl MJ, Fisher AT, Slack JF) College Station, TX, *Ocean Drilling Program*, **139**, 695–717.

Davis EE, Lister CRB (1974) Fundamentals of ridge crest topography. *Earth and Planetary Science Letters*, **21**, 405–13.

Davis EE, Villinger H (1992) Tectonic and thermal structure of the Middle Valley sedimented rift, northern Juan de Fuca Ridge. In: *Proc. ODP, Init. Repts.* (eds Davis EE, Mottl M, Fisher AT) College Station, TX, *Ocean Drilling Program*, **139**, 9–41.

Davis EE, Wang K (1994) Present and past temperatures of sediments at Site 857, Middle Valley, northern Juan de Fuca Ridge. In: *Proc. ODP, Sci. Res.* (eds Davis EE, Mottl MJ, Fisher AT, Slack JF) College Station, TX, *Ocean Drilling Program*, **139**, 565–72.

Davis EE, Chapman DS, Forster C, Villinger H (1989) Heat-flow variations correlated with buried basement topography on the Juan de Fuca Ridge flank. *Nature*, **342**, 533–7.

Davis EE, Chapman DS, Mottl MJ, Bentkowski WJ, Dadey K, Forster C, Harris R, Nagihara S, Rohr K, Wheat G, Whiticar M (1992) FlankFlux: an experiment to study the nature of hydrothermal circulation in young oceanic crust. *Canadian Journal of Earth Sciences*, **29**, 925–52.

Davis EE, Villinger H, Macdonald RD, Meldrum RD, Grigel J (1997a) A robust rapid-response probe for measuring bottom-hole temperatures in deep-ocean boreholes. *Marine Geophysical Researches*, **19**, 267–81.

Davis EE, Wang K, He J, Chapman DS, Villinger H, Rosenberger A (1997b) An unequivocal case for high Nusselt-number hydrothermal convection in sediment-buried igneous oceanic crust. *Earth and Planetary Science Letters*, **146**, 137–50.

Davis EE, Chapman DS, Wang K, Villinger H, Fisher AT, Robinson SW, Grigel J, Pribnow D, Stein J, Becker K (1999) Regional heat-flow variations across the sedimented Juan de Fuca Ridge eastern flank: constraints on lithospheric cooling and lateral hydrothermal heat transport. *Journal of Geophysical Research*, **104**, 17, 675–88.

Davis EE, Wang K, Becker K, Thomson RE, Yashayaev I (2003) Deep-ocean temperature variations and implications for errors in seafloor heat flow determinations. *Journal of Geophysical Research*, **108**, 2034. doi:2110.1029/2001JB001695.

Elder JW (1965) Physical processes in geothermal areas. In: *Terrestrial Heat Flow* (ed Lee WHK) Washington, DC, *American Geophysics Union*, **8**, 211–39.

Elderfield H, Wheat CG, Mottl MJ, Monnin C, Spiro B (1999) Fluid and geochemical transport through oceanic crust: a transect across the eastern flank of the Juan de Fuca Ridge. *Earth and Planetary Science Letters*, **172**, 151–65.

Fisher AT, Becker K (1993) A guide for ODP tools for downhole measurements, Technical note 10, doi: 10.2973/odp.tn.10. 1993. Available at: http://www-odp.tamu.edu/publications/tnotes/tn10/10toc.html (accessed 31 December 2009).

Fisher AT, Becker K (2000) Channelized fluid flow in oceanic crust reconciles heat-flow and permeability data. *Nature*, **403**, 71–4.

Fisher AT, Becker K, Narasimhan TN, Langseth MG, Mottl MJ (1990) Passive, off-axis convection on the southern flank of the Costa Rica Rift. *Journal of Geophysical Research*, **95**, 9343–70.

Fisher AT, Fischer K, Lavoie D, Langseth M, Xu J (1994) Hydrogeological and geotechnical properties of shallow sediments at Middle Valley, northern Juan de Fuca Ridge. In: *Proc. ODP, Sci. Res.* (eds Mottl MJ, Davis EE, Fisher AT, Slack JF) College Station, TX, *Ocean Drilling Program*, **139**, 627–48.

Fisher AT, Becker K, Davis EE (1997) The permeability of young oceanic crust east of Juan de Fuca Ridge determined using borehole thermal measurements. *Geophysical Research Letters*, **24**, 1311–4.

Fisher AT, Davis EE, Hutnak M, Spiess V, Zühlsdorff L, Cherkaoui A, Christiansen L, Edwards KM, Macdonald R, Villinger H, Mottl MJ, Wheat CG, Becker K (2003a) Hydrothermal recharge and discharge across 50 km guided by seamounts on a young ridge flank. *Nature*, **421**, 618–21.

Fisher AT, Stein CA, Harris RN, Wang K, Silver EA, Pfender M, Hutnak M, Cherkaoui A, Bodzin R, Villinger H (2003b) Abrupt thermal transition reveals hydrothermal boundary and role of seamounts within the Cocos Plate. *Geophysical Research Letters*, **30**, 1550, doi:1510.1029/2002GL016766.

Fisher AT, Villinger H, Heesemann M (2007) *User Manual for the Third-Generation, Advanced Piston Corer Temperature tool (APCT-3)*. Integrated Ocean Drilling Program, College Station, TX.

Fisher AT, Davis EE, Becker K (2008) Borehole-to-borehole hydrologic response across 2.4 km in the upper oceanic crust: implications for crustal-scale properties. *Journal of Geophysical Research*, **113**, B07106, doi:10.1029/2007JB005447.

Foucher J-P, Henry P, Harmegnies F (1997) Long-term observations of pressure and temperature in Hole 948D, Barbados accretionary prism. In: *Proc. ODP, Sci. Res.* (eds Ogawa Y, Shipley T, Blum P, Bahr J) College Station, TX, *Ocean Drilling Program*, **156**, 239–46.

Fukasawa M, Freeland H, Perkin R, Wantanabe T, Uchida H, Nishina A (2003) Bottom water warming in the North Pacific Ocean. *Nature*, **427**, 825–7.

Gieskes J, Kastner M, Einsele G, Kelts K, Niemitz J (1982) Hydrothermal activity in the Guayman Basin, Gulf of California, a synthesis. In: *Init. Repts., DSDP* (eds Curray J, Moore D), U. S. Govt. Printing Office, Washington, D. C., **64**, 1159–68.

Goto S, Yamano M, Kinoshita H (2005) Thermal response of sediment with vertical fluid flow to periodic temperature variation at the surface. *Journal of Geophysical Research*, **110**, B01106, doi:10.1029/2004JB003419.

Hamamoto H, Yamano M, Goto S (2005) Heat flow measurement in shallow seas through long-term temperature monitoring. *Geophysical Research Letters*, **32**, L21311.

Harris RN, Chapman DS (2004) Deep-seated oceanic heat flow, heat deficits, and hydrothermal circulation. In: *Hydrogeology of the Oceanic Lithosphere* (eds Davis EE, Elderfield H), pp. 311–36. Cambridge University Press, Cambridge, UK.

Harris RN, Von Herzen RP, McNutt MK, Garven G, Jordahl K (2000) Submarine hydrogeology of the Hawaiian archipelagic apron, Part 1, Heat flow patterns north of Oahu and Maro Reef. *Journal of Geophysical Research*, **105**, 21, 353–69.

Hartmann A, Villinger H (2002) Inversion of marine heat flow measurements by expansion of the temperature decay function. *Geophysical Journal International*, **148**, 628–36.

Horai K, Von Herzen RP (1985) Measurement of heat flow on Leg 86 of the Deep Sea Drilling Project. In: *Init. Repts., DSDP* (eds Heath GR, Burckle LH), U. S. Govt. Printing Office, Washington, D. C., **86**, 759–77.

von Huene R, Ranero CR, Wienrebe W, Hinz K (2000) Quarternary convergent margin tectonics of Costa Rica, segmentation of the Cocos Plate, and Central American Volcanism. *Tectonics*, **19**, 314–34.

Hutnak M, Fisher AT (2007) The influence of sedimentation, local and regional hydrothermal circulation, and thermal rebound on measurements of heat flux from young seafloor. *Journal of Geophysical Research*, **112**, B12101, doi:10.1029/2007JB005022.

Hutnak M, Fisher AT, Zühlsdorff L, Spiess V, Stauffer P, Gable CW (2006) Hydrothermal recharge and discharge guided by basement outcrops on 0.7-3.6 Ma seafloor east of the Juan de Fuca Ridge: observations and numerical models. *Geochemistry, Geophysics, and Geosystems*, **7**, Q07O02, doi:10.1029/2006GC001242.

Hutnak M, Fisher AT, Stein CA, Harris R, Wang K, Silver E, Spinelli G, Pfender M, Villinger H, MacKnight R, Costa Pisani P, DeShon H, Diamente C (2007) The thermal state of 18-24 Ma upper lithosphere subducting below the Nicoya Peninsula, northern Costa Rica margin. In: *MARGINS Theoretical Institute: SIEZE Volume* (eds Dixon T, Moore C, Silver E, Stein S, Furlong K, Brown K), pp. 86–122. Columbia University Press, New York.

Hutnak M, Fisher AT, Harris R, Stein C, Wang K, Spinelli G, Schindler M, Villinger H, Silver E (2008) Large heat and fluid fluxes driven through mid-plate outcrops on ocean crust. *Nature Geoscience*, **1**, 611–4.

Hyndman RD, Von Herzen RP, Erickson AJ, Jolivet J (1976) Heat flow measurements in deep crustal holes on the Mid-Atlantic Ridge. *Journal of Geophysical Research*, **81**, 4053–60.

Hyndman RD, Davis EE, Wright JA (1979) The measurement of marine geothermal heat flow by a multipenetration probe with digital acoustic telemetry and in situ conductivity. *Marine Geophysical Researches*, **4**, 181–205.

Johnson HP, Hutnak M (1996) Conductive heat flow measured in unsedimented regions of the seafloor. *Transactions, American Geophysical Union*, **77**, 321–4.

Kastner M (1982) Evidence for two distinct hydrothermal systems in the Gulf of California. In: *Init. Repts., DSDP* (eds Curray J,

Moore D) U. S. Govt. Printing Office, Washington, D. C., **64**, 529–42.
Kinoshita M, Matsubayashi O, Von Herzen RP (1996) Sub-bottom temperatrue anomalies detected by long-term temperatrue monitoring at the TAG hydrothermal mound. *Geophysical Research Letters*, **23**, 3467–70.
Langseth M, Becker K (1994) Structure of igneous basement at Sites 857 and 858 based on Leg 139 downhole logging. In: *Proc. ODP, Sci. Res.* (eds Davis EE, Mottl MJ, Fisher AT, Slack JF) College Station, TX, *Ocean Drilling Program*, **139**, 573–83.
Langseth MG, Herman B (1981) Heat transfer in the oceanic crust of the Brazil Basin. *Journal of Geophysical Research*, **86**, 10805–19.
Langseth MG, Silver EA (1996) The Nicoya convergent margin – a region of exceptionally low heat flow. *Geophysical Research Letters*, **23**, 891–4.
Langseth MG, Grim PJ, Ewing M (1965) Heat-flow measurements in the east Pacific Ocean. *Journal of Geophysical Research*, **70**, 367–80.
Langseth MG, LePichon X, Ewing M (1966) Crustal structure of the midocean ridges, 5, heat flow through the Atlantic Ocean floor and convection currents. *Journal of Geophysical Research*, **71**, 5321–55.
Larson RL, Fisher AT, Jarrard R, Becker K (1993) Highly permeable and layered Jurassic oceanic crust in the western Pacific. *Earth and Planetary Science Letters*, **119**, 71–83.
Lister CRB (1972) On the thermal balance of a mid-ocean ridge. *Geophysical Journal of the Royal Astronomical Society*, **26**, 515–35.
Lonsdale P, Becker K (1985) Hydrothermal plumes, hot springs, and conductive heat flow in the southern trough of Guaymas Basin. *Earth and Planetary Science Letters*, **73**, 211–25.
Louden KE, Wright JA (1989) Marine heat flow data: a new compilation of observations and brief review of its analysis. In: *Handbook of Seafloor Heat Flow* (eds Wright JA, Louden KE), pp. 3–67. CRC Press, Boca Raton, FL.
Lu N, Ge S (1996) Effect of horizontal heat and fluid flow on the vertical temperature distribution in a semiconfining layer. *Water Resources Research*, **32**, 1449–53.
McKenzie D (1967) Some remarks on heat flow and gravity anomalies. *Journal of Geophysical Research*, **72**, 6261–73.
McNutt MK (1995) Marine geodynamics: depth-age revisited. *Reviews of Geophysics*, **33**, 413–8.
Meschede M, Barckhausen U, Worm H-U (1998) Extinct spreading on the Cocos Ridge. *Terra Nova*, **10**, 211–6.
Mottl M (2003) Partitioning of energy and mass fluxes between mid-ocean ridge axes and flanks at high and low temperature. In: *Energy and Mass Transfer in Submarine Hydrothermal Systems* (eds Halbach P, Tunnicliffe V, Hein J), pp. 271–86. University Press, Berlin, Germany, Dahlem, DWR 89.
Mottl MJ, Wheat CG, Baker E, Becker N, Davis E, Feeley R, Grehan A, Kadko D, Lilley M, Massoth G, Moyer C, Sansone F (1998) Warm springs discovered on 3.5 Ma oceanic crust, eastern flank of the Juan de Fuca Ridge. *Geology*, **26**, 51–4.
Parker RL, Oldenberg DW (1973) Thermal model of ocean ridges. *Nature*, **242**, 137–9.
Parsons B, Sclater JG (1977) An analysis of the variation of ocean floor bathymetry and heat flow with age. *Journal of Geophysical Research*, **82**, 803–29.
Pfender M, Villinger H (2002) Miniaturized data loggers for deep sea sediment temperature gradient measurements. *Marine Geology*, **186**, 557–70.
Pribnow DFC, Davis EE, Fisher AT (2000) Borehole heat flow along the eastern flank of the Juan de Fuca Ridge, including effects of anisotropy and temperature dependence of sediment thermal conductivity. *Journal of Geophysical Research*, **105**, 13449–56.
Ranero CR, von Huene R (2000) Subduction erosion along the Middle America convergent margin. *Nature*, **404**, 748–52.
Revelle R, Maxwell AE (1952) Heat flow through the ocean floor. *Nature*, **170**, 199–200.
Rosenberg N, Fisher AT, Stein J (2000) Large-scale lateral heat and fluid transport in the seafloor: revisiting the well-mixed aquifer model. *Earth and Planetary Science Letters*, **182**, 93–101.
Sclater JG (2004) Variability of heat flux through the seafloor: discovery of hydrothermal circulation in oceanic crust. In: *Hydrogeology of the Oceanic Lithosphere* (eds Davis EE, Elderfield H), pp. 3–27. Cambridge University Press, Cambridge, UK.
Sclater JG, Jaupart C, Galson D (1980) The heat flow through oceanic and continental crust and the heat loss of the earth. *Reviews of Geophysics and Space Physics*, **18**, 269–311.
Spinelli GA, Giambalvo EG, Fisher AT (2004) Hydrologic properties and distribution of sediments. In: *Hydrogeology of the Oceanic Lithosphere* (eds Davis EE, Elderfield H), pp. 151–88. Cambridge University Press, Cambridge, UK.
Stein JS, Fisher AT (2001) Multiple scales of hydrothermal circulation in Middle Valley, northern Juan de Fuca Ridge: physical constraints and geologic models. *Journal of Geophysical Research*, **106**, 8563–80.
Stein CA, Stein S (1992) A model for the global variation in oceanic depth and heat flow with lithospheric age. *Nature*, **359**, 123–37.
Stein C, Stein S (1994) Constraints on hydrothermal heat flux through the oceanic lithosphere from global heat flow. *Journal of Geophysical Research*, **99**, 3081–95.
Stein CA, Stein S, Pelayo AM (1995) Heat flow and hydrothermal circulation. In: *Seafloor Hydrothermal Systems: Physical, Chemical, Biological and Geological Interactions* (eds Humphris SE, Zierenberg RA, Mullineaux LS, Thompson RE) American Geophysical Union, Washington, D. C., **91**, 425–45.
Stein J, Fisher AT, Langseth M, Jin W, Iturrino G, Davis E (1998) Fine-scale heat flow, shallow heat sources, and decoupled circulation systems at two seafloor hydrothermal sites, Middle Valley, northern Juan de Fuca Ridge. *Geology*, **26**, 1115–1118.
Thomson RE, Davis EE, Burd BJ (1995) Hydrothermal venting and geothermal heating in Cascadia Basin. *Journal of Geophysical Research*, **100**, 6121–41.
Uyeda S, Horai K (1980) Heat flow measurements on Deep Sea Drilling Project Leg 60. In: *Init. Repts., DSDP* (eds Hussong D, Uyeda S), U. S. Govt. Printing Office, Washington, D. C., **60**, 789–800.
Vacquier V, Sclater JG, Corry CE (1967) Studies in the thermal state of the earth, the 21st paper: heat-flow, Eastern Pacific. *Bulletin of the Earthquake Research Institute*, **45**, 375–93.
Veirs SR, McDuff RE, Lilley MD, Delaney JR (1999) Locating hydrothermal vents by detecting buoyant, advected plumes. *Journal of Geophysical Research*, **104**, 29.
Villinger H, Davis EE (1987) A new reduction algorithm for marine heat-flow measurements. *Journal of Geophysical Research*, **92**, 12846–56.
Villinger H, Grevemeyer I, Kaul N, Hauschild J, Pfender M (2002) Hydrothermal heat flux through aged oceanic crust: where does the heat escape? *Earth and Planetary Science Letters*, **202**, 159–70.

Von Herzen RP (2004) Geothermal evidence for continuing hydrothermal circulation in older (>60 Ma) ocean crust. In: *Hydrogeology of the Oceanic Lithosphere* (eds Davis EE, Elderfield H), pp. 414–50. Cambridge University Press, Cambridge, UK.

Von Herzen RP, Maxwell AE (1959) The measurement of thermal conductivity of deep-sea sediments by a needle probe method. *Journal of Geophysical Research*, **64**, 1557–63.

Von Herzen R, Uyeda S (1963) Heat flow through the eastern Pacific floor. *Journal of Geophysical Research*, **68**, 4219–50.

Von Herzen R, Davis EE, Fisher AT, Stein CA, Pollack HN (2005) Comments on ''Earth's heat flux revised and linked to chemistry'' by A. M. Hoffmeister and R. E. Criss. *Tectonophysics*, **409**, 193–8.

Wang K, Davis EE (1992) Thermal effects of marine sedimentation in hydrothermally active areas. *Geophysical Journal International*, **110**, 70–8.

Wheat CG, Fisher AT (2007) Seawater recharge along an eastern bounding fault in Middle Valley, northern Juan de Fuca Ridge. *Geophysical Research Letters*, **34**, L20602, doi:10.1029/2007GL031347.

Wheat CG, Mottl MJ (1994) Hydrothermal circulation, Juan de Fuca Ridge eastern flank: factors controlling basement water composition. *Journal of Geophysical Research*, **99**, 3067–80.

Wheat CG, Mottl M (2000) Composition of pore and spring waters from Baby Bare: global implications of geochemical fluxes from a ridge flank hydrothermal system. *Geochimica Cosmochimica Acta*, **64**, 629–42.

Wheat CG, Elderfield H, Mottl MJ, Monnin C (2000) Chemical composition of basement fluids within an oceanic ridge flank: implications for along-strike and across-strike hydrothermal circulation. *Journal of Geophysical Research*, **105**, 13437–47.

Wheat CG, Mottl MJ, Fisher AT, Kadko D, Davis EE, Baker E (2004) Heat and fluid flow through a basaltic outcrop on a ridge flank. *Geochemistry, Geophysics and. Geosystems*, **5**, Q12006, doi:10.1029/2004GC000700.

Wilson DS (1993) Confidence intervals for motion and deformation of the Juan de Fuca plate. *Journal of Geophysical Research*, **98**, 16.

Wolery TJ, Sleep NH (1975) Hydrothermal reaction at mid-ocean ridges: some implications and constraints. *EOS, Transactions, American Geophysical Union*, **56**, 1073.

Zühlsdorff L, Hutnak M, Fisher AT, Spiess V, Davis EE, Nedimovic M, Carbotte S, Villinger H, Becker K (2005) Site Surveys related to IODP Expedition 301: ImageFlux (SO149) and RetroFlux (TN116) expeditions and earlier studies. In: *Proc. IODP* (eds Fisher AT, Urabe T, Klaus A) College Station, TX, *Integrated Ocean Drilling Program, Expedition* **301**, doi:10.2204/iodp.proc.2301.2102.2005.